Simulated global tropospheric PAN:
Its transport and impact on NO_x

W. J. Moxim and H. Levy II

Geophysical Fluid Dynamics Laboratory, NOAA, Princeton, New Jersey

P. S. Kasibhatla[1]

School of Earth and Atmospheric Sciences, Georgia Institute of Technology, Atlanta, Georgia

Abstract. Using the 11-level Geophysical Fluid Dynamics Laboratory (GFDL) global chemical transport model (GCTM) with all known sources of tropospheric NO_x, we simulate the global tropospheric distribution of peroxyacetyl nitrate (PAN) and quantify its impact on tropospheric NO_x. The model's global distribution of PAN is in reasonable agreement with most available observations. In the atmospheric boundary layer, PAN is concentrated over the continental sites of NO_x emissions, primarily the midlatitudes in the northern hemisphere and the subtropics in the southern hemisphere. PAN is distributed relatively zonally throughout the free troposphere of the northern hemisphere, with the maximum levels found in the coldest regions, while in the southern hemisphere the maximum PAN levels are found in an equator to $30°S$ belt stretching from South America to Australia. Overall, the simulated three-dimensional fields of seasonal PAN are a result of the interaction of the type of transport meteorology (convective or synoptic scale storms) occurring in the PAN formation regions and PAN's temperature-dependent lifetime. We find the impact of PAN chemistry on NO_x to be rather subtle. The magnitude and the seasonal cycle of the global tropospheric integral of NO_x, which has its maximum in January and the formation of HNO_3 as its dominant loss path, are barely affected by the inclusion of PAN chemistry, however PAN, as a result of its temperature sensitivity and transport, regionally provides an efficient mechanism for redistributing NO_x far from its source areas. With the inclusion of PAN chemistry, monthly mean NO_x concentrations increase by up to a factor of 5 in the remote lower troposphere and show a spring maximum over areas of the North Atlantic and North Pacific Oceans. In contrast, PAN has only a minor impact in the upper half of the troposphere ($\pm 10\%$). Examining local time series of NO_x and PAN, the monthly mean mixing ratios in remote regions are shown to be composed of numerous short-term (1-2 days) large magnitude events. These episodes are large enough to potentially result in ozone production even when the monthly mean NO_x values are in the ozone destruction range. While both the direct transport of NO_x and its indirect transport as PAN contribute to the elevated NO_x episodes over the remote extratropical oceans, events over the remote subtropical oceans are dominated by midtropospheric PAN that sinks anticyclonically equatorward and decomposes to NO_x in the warmer air.

1. Introduction

Nitrogen oxides (NO_x), through their control, both direct and indirect, of the chemical production of OH and ozone [*Levy*, 1971; *Chameides and Walker*, 1973; *Crutzen*, 1974; see *Crutzen*, 1988, for a detailed summary] are expected to play a major role in determining the global reactivity of the troposphere. As expected, the greatest concentrations of NO_x are found in or near the major continental combustion, biomass, and biogenic surface source regions. NO_x that is transported from its source domain is typically subject to a relatively short chemical lifetime of the order of a few days in the atmospheric boundary layer (ABL). This is a result of its

daytime conversion to HNO_3 by OH and the complex aerosol-dependent tropospheric nighttime reaction of NO_2 with O_3 and the subsequent heterogeneous conversion of N_2O_5 to HNO_3 on sulfate aerosols. In view of this fact it is interesting to note that the three-dimensional model simulations of *Moxim et al.* [1994] and H. Levy II et al. (manuscript in preparation, 1996) depict winter and spring monthly mean NO_x mixing ratios as high as 50 to 80 parts per trillion by volume (pptv) in the remote ocean regions of the lower troposphere, thousands of kilometers from large continental source regions. Depending on ozone concentrations, these values place NO_x near the balance point between net chemical production and net chemical destruction of O_3 (see *Fehsenfeld et al.* [1988] for a recent discussion of background NO_x measurements; *Levy et al.* [1985], *Lin et al.* [1988], *Sillman et al.* [1990], and A. Klonecki and H. Levy II (manuscript in preparation, 1996) for discussions of the dependence of ozone chemistry on NO_x concentration; *Liu et al.* [1983], *Chameides et. al.* [1987], *Carroll et al.* [1990], *Ridley et al.*, [1992], and *Liu et al.* [1992] for discussions of ozone budgets over the Pacific).

---

[1] Formerly visiting scientist at Geophysical Fluid Dynamics Laboratory, Princeton University, Princeton, New Jersey.

A potential explanation for these high values of remote NO_x may be found in the formation, transport, and loss of PAN. Both measurements [e.g., *Singh et al.*, 1986, 1990, 1992, 1994] and a three-dimensional GCTM study [*Kasibhatla et al.*, 1993] have shown that in the free troposphere, PAN is a major component of reactive nitrogen compounds (NO_y). This chemical specie is unique in terms of atmospheric transport in that its lifetime is strongly controlled by meteorology due to PAN's high sensitivity to typical tropospheric temperatures (i.e., 4°C ~ 1 day lifetime, -12°C ~ 20 days, -30°C ~ 100 days), which originally led to the speculation that PAN could serve as a stable form of NO_x that would be available for long-range transport from source regions [*Crutzen*, 1979]. Also, it has been hypothesized that the formation of PAN from background NO_x and hydrocarbons in the free troposphere would serve as an additional temporary reservoir for NO_x and that PAN, either as a free tropospheric reservoir or as a temporary transport surrogate for NO_x, may control the concentrations of NO_x away from its source regions and thereby control the chemical production of O_3 in much of the troposphere [*Singh and Hanst*, 1981]. In addition, it has also been argued that the spring maximum observed in PAN in the northern high latitudes is related to and at least partly responsible for the observed spring maximum in tropospheric O_3 [*Penkett and Brice*, 1986].

While investigating the impact of fossil fuel combustion emissions on the distribution of reactive nitrogen compounds (NO_y), *Kasibhatla et al.* [1993] noted that if PAN chemistry was neglected, the amount of NO_x in remote regions was underestimated. In this study we will use the GFDL GCTM with all known sources of NO_x to explore in detail PAN's role in the global distribution of NO_x. To accomplish this, we will evaluate our simulated PAN distribution by comparing it with available observations and then discuss its latitudinal, longitudinal, and seasonal behavior. Next, global tropospheric and zonal average monthly integrals for NO_x emissions, PAN production and loss, net PAN chemistry, and PAN itself are used to examine the complex role played by chemistry, temperature, and transport in the distribution of PAN. Finally, utilizing various analysis methods, we examine the important issue of the seasonal impact of PAN on global, regional and local NO_x levels, as well as the type of meteorological transport paths affecting remote regions.

2. Model Description

For our study we explicitly separate reactive nitrogen [NO_y] into three classes of transported species: nitrogen oxides (NO + NO_2 + NO_3 + N_2O_5), nitric acid (HNO_3), and PAN. The conservation equations for their mixing ratios are integrated globally, using the GFDL three-dimensional GCTM, until all tropospheric distributions are equilibrated. The GCTM is driven by 6-hour time-averaged winds and a consistent total column precipitation field that was generated by a parent general circulation model (GCM) integrated for 1 year without diurnal insolation (see section 2 of *Mahlman and Moxim* [1978] for a summary and *Manabe et al.* [1974] and *Manabe and Holloway* [1975] for details). Therefore the GCTM cannot realistically simulate atmospheric fluctuations with periods shorter than 6 hours or examine interannual variability. Both the parent GCM and the GCTM have the same resolution, a horizontal grid size of ~265 km, and 11 vertical levels at standard pressures of 990, 940, 835, 685,

500, 315, 190, 110, 65, 38, and 10 mbar. The GCTM includes parameterizations designed to incorporate the effects of horizontal subgrid scale transport, as well as vertical mixing by dry and moist convection (for details see Appendix A, *Levy et al.* [1982] and section 2, *Kasibhatla et al.* [1993]).

Six distinct previously described sources of reactive nitrogen are incorporated in the model: anthropogenic emissions of NO_x from surface fossil fuel combustion (21.3 Tg N/yr, *Levy and Moxim* [1989], updated with the GEIA project, Benkovitz et al. [1996]), aircraft traffic (0.45 Tg N/yr, *Kasibhatla* [1993]), biomass burning (8.5 Tg N/yr, *Levy et al.* [1991]), natural or primarily natural NO_x emissions from soil (5.5 Tg N/yr, *Yienger and Levy* [1995]), injection of stratospheric NO_x (0.6 Tg N/yr, *Kasibhatla et al.* [1991]), and lightning discharge (3.0 Tg N/yr, *Levy et al.* [1996]).

Dry deposition fluxes of NO_x, HNO_3 and PAN over land as well as HNO_3 over oceans, ice, and snow are calculated on the basis of assumption of a balance between surface deposition and the turbulent flux in the bottom half of the lowest model level [see *Kasibhatla et al.*, 1993, equation (2)], and dry deposition velocities used in the model reflect measured deposition velocities of individual reactive nitrogen species [see *Kasibhatla et al.*, 1993, section 3]. The removal of HNO_3 by precipitation is calculated using the local precipitation rate, and the wet removal tendency is proportional to the local tracer mixing ratio (see section 2, *Kasibhatla et al.* [1991] for details).

Daytime chemical production and loss rates among NO_x, HNO_3 and PAN are calculated off-line using a standard O_3, NO_x, CO, CH_4, HxOy, chemical scheme (e.g., *Chameides and Tan*, 1981) and are carried in the GCTM as temporally-varying, two-dimensional zonal fields [see section 3 in *Kasibhatla et al.* (1991) and section 2 in *Kasibhatla et al.* (1993) for details]. The nighttime heterogeneous conversion of NO_2 to HNO_3 is also calculated off-line and carried as a monthly varying three-dimensional field [see H. Levy II et al. (manuscript in preparation, 1996)]. The thermal decomposition rate of PAN, however, is calculated on-line as a function of the model local grid point temperature.

In our model, as described by *Kasibhatla et al.* [1993], PAN formation occurs via the reaction of peroxyacetyl radical (PAC) with NO_2. The PAC, in turn, is generated by the reaction of nonmethane hydrocarbons (NMHC) with OH (see *Kasibhatla et al.* [1991], section 3, for details). NMHC concentrations used to calculate PAN formation rates are specified according to model calculated, two-dimensional, monthly varying ethane and propane fields from *Kanakidou et al.* [1991]. Over continents, short lived natural hydrocarbons, such as isoprene, can contribute significantly to PAN formation [e.g., *Trainer et al.*, 1991]. To take this into account, we have adjusted NMHC levels so as to approximately reproduce observed summer PAN levels at a rural site in the eastern United States (Scotia, Pennsylvania) as well as PAN fractions measured during periods of east winds at Boulder, Colorado, in February (M. P. Buhr, private communication, 1992), and at Egbert, Ontario, in April [*Shepson et al.*, 1992]. To accomplish this, we have increased NMHC concentrations over land in the bottom three model levels between 30°N and 65°N by a factor of 3 in summer and by a factor of 1.5 in spring and fall, relative to the two-dimensional fields of *Kanakidou et al.* [1991]. South of 30°N, NMHC concentrations over land in the bottom three model levels have been adjusted so that, throughout the year, they are approximately equal to summer,

lower tropospheric NMHC concentrations over land specified between 30°N and 65°N. The rational for this stems from studies [e.g., *Chameides et al.*, 1992] which find that on an OH reactivity based scale, surface hydrocarbon levels observed over remote tropical forests are comparable to those in the rural areas of the eastern United States during summer.

We assert that our approach of treating PAN chemistry in a global, three-dimensional transport model offers a reasonable compromise between approaches which neglect PAN chemistry entirely in three-dimensional model simulations [e.g., *Penner et al.*, 1991] and approaches which treat PAN chemistry more comprehensively, albeit in a two-dimensional transport model framework [e.g., *Kanakidou et al.*, 1991].

3. PAN Simulation

All model integrations were initialized with uniform mixing ratios of 1 pptv of NO_x, HNO_3, and PAN and run for a period of 16 months from a model start-up date of October 1. Tropospheric sources and sinks are in approximate balance after the initial 2 to 3 months. All discussions are based on the results from the last 12 months.

3.1. Comparison With Observations

When comparing observations and model data, one should keep in mind that both have inherent weaknesses. While the GFDL GCTM provides a wealth of tracer data available every six hours at 7140 horizontal grid points over 11 vertical levels allowing a large range of analysis, basic model assumptions and parameterizations introduce some shortcomings into its chemistry, transport meteorology, and sources. Also, as a result of three-dimensional transport wind fields being available from only one GCM model year, the GCTM cannot analyze interannual variability. On the other hand, observations of chemical species have their own problem in that they are usually sparse in space and time and even intensive measurement campaigns have only a 1- to 2- month duration, precluding diagnosis of seasonal variations. As is shown in section 4.3, tropospheric tracers from the subtropics to high latitudes can exhibit large fluctuations on a synoptic timescale of several days. Any short-term measurement could depict values which vary greatly from the actual monthly mean. Therefore limited observations alone cannot provide a comprehensive global climatology that is sensitive to the day-to-day and seasonal variations in tropospheric circulation.

In Tables 1 and 2 our model simulation is compared with the available published observations of PAN. Table 1 presents the more complete data sets generated during the Arctic Boundary Layer Expedition (ABLE) 3A and 3B, the Mauna Loa Observatory Photochemistry Experiment (MLOPEX), the Pacific Exploratory Mission in the western North Pacific (PEMWest A) and the Transport and Atmospheric Chemistry near the Equator-Atlantic (TRACE A) studies, while Table 2 depicts less detailed data sets (e.g., cruises and single aircraft transit flights). For all comparisons we present the model's mean, median (med), standard deviation (s.d.) and the 50th percentile range (50%). This was accomplished by analyzing model data at a given grid box containing the measurement site and altitude (i.e., Mauna Loa), or in the case of aircraft data, all the grid boxes that a flight path passed through over the given time period. For the measurements presented in Table 1, we produced the same statistics over all available

observations (N), while for the sparser data of Table 2, we simply give the range of the data (depicted by brackets). The binning of observed data by altitude was dictated by the model's vertical standard pressure layers as follows: 190 mbar implies a (150 to 241 mbar) range; 315 (241-412); 500 (412-607; 685 (607-773); 835 (773-902) and the model surface (sfc) is 990 mbar.

The two dominant qualitative features of PAN's tropospheric distribution are clearly present in both the available observations and the numerical simulation: (1) While PAN is found throughout the global troposphere, there is a sharp gradient, as seen in the surface data in Table 2, between the two hemispheres with most PAN found in the northern hemisphere (NH). (2) As described in the introduction, the key role played by temperature is noted by PAN's increase with height from the warmer surface to the colder free troposphere as well as from tropics to high latitudes in the lower troposphere.

Examining Tables 1 and 2 more quantitatively, we find that overall, the model simulations and observations are in general good agreement in both vertical structure and seasonality. Most importantly, the model performs reasonably well in remote oceanic regions where it will be shown that PAN plays a critical role in determining NO_x levels. However, there are some discrepancies in the midtroposphere of the NH during the summer and the southern hemisphere (SH) during its spring and Alert, Canada, during winter:

1. The ABLE 3B measurements over eastern Canada during summer are substantially higher in the mean than our model simulation, especially at 685 mbar (factor of 2.4). One possibility for this discrepancy is that 13 of the 18 recording flights were impacted by forest fire smoke [*Singh et al.*, 1994] which may have help produce the observed PAN mixing ratios as indicated by the large standard deviations.

2. The TRACE A PAN mixing ratios in the SH free troposphere during September-October are much higher (~factor of 2) over both the land and the ocean than those indicated by the model, although the GCTM does produce the observed land-sea gradient. These observations, however, were obtained during the SH biomass burning season with a bias towards deep convective events, while the GCTM samples every six hours during times of subsidence as well as convection. It is also possible that our specification of nonmethane hydrocarbons in this region may have been too low and our simulated convection too weak during this period.

3. The high PAN simulated mixing ratios at Alert during winter probably are a result of subsidence being too strong. Also, horizontal advection may be too weak, since the GCTM's grid tends to inhibit cross-polar flow.

3.2. Simulated PAN Distribution

Having examined the available measurements of PAN, we will now attempt to fill in the observational voids utilizing our GCTM results. To obtain an overall view of the structure and seasonality of PAN, we first display the zonally averaged two-dimensional profiles of PAN shown in Figure 1, which confirm those principle features of its distribution that were suggested by Tables 1 and 2.

1. Most tropospheric PAN is found in the NH with the greatest amounts in middle and high latitudes.

2. In general, PAN tends to accumulate during winter and spring in the NH extratropical troposphere when temperatures are lowest and PAN has the longest lifetime. Note that during

Table 1. Statistical Comparison of Model Simulation and Observations

Region	Observations	Pressure	Measurement				Model Result		
			Mean/Med	50%	s.d.	N	Mean/Med	50%	s.d.
ABLE 3A[a]	July-Aug.	500	103/37	(28-166)	115	201	110/109	(83-137)	40
(Alaska)		685	49/18	(9-34)	75	182	55/51	(28-80)	35
		835	14/5	(3-12)	22	91	23/21	(10-33)	16
ABLE 3B[b]	July-Aug.	500	219/234	(31-331)	189	161	141/137	(111-166)	45
eastern Canada		685	230/201	(30-350)	218	84	95/88	(61-119)	48
North of 50°N		835	91/68	(50-121)	72	53	64/54	(34-82)	45
MLOPEX[c]	winter	685	45/42	23-57)	30	109	44/22	(5-66)	56
(Mauna Loa)	May 1-June 4 1988		19/15	(7-24)	14	37	38/36	(14-56)	27
	Apr.-May 13 1992		47/38	(18-66)	34	103	59/53	(23-70)	50
	summer		15/11	(7-15)	12	52	18/18	(10-24)	9
	fall		18/14	(11-23)	12	72	29/15	(8-44)	30
PEM-West A[d]	Sept.-Oct.	190	72/62	(25-106)	54	85	60/59	(45-73)	24
(W. Pacific Ocean)		315	73/47	(23-121)	58	106	100/97	(67-129)	48
> 30°N		500	111/98	(40-157)	85	71	163/153	(95-219)	90
		685	129/125	(26-194)	97	31	168/154	(65-245)	122
PEM-West A[d]	Sept.-Oct.	190	22/21	(17-26)	8	48	27/22	(15-33)	19
(W. Pacific Ocean)		315	29/17	(11-28)	34	240	27/24	(17-33)	15
"0° - 25°N"		500	30/19	(15-28)	32	116	46/34	(21-59)	37
		685	11/8	(2-12)	20	79	26/13	(6-29)	33
TRACE A[e]	Sept.-Oct.	190	224/213	(164-283)	86	204	98/85	(62-113)	48
(S. Atlantic Ocean)		315	295/262	(173-354)	224	474	115/103	(76-140)	59
"0° - 30°S"		500	291/250	(213-351)	155	80	139/126	(94-173)	66
		685	278/115	(29-427)	322	125	83/63	(42-100)	66
TRACE A[e]	Sept.-Oct.	190	343/252	(163-414)	276	56	112/90	(60-131)	93
Land		315	318/246	(180-372)	290	290	150/128	(91-183)	92
(S.America		500	387/312	(218-472)	281	182	181/164	(118-220)	101
and Africa)		685	644/398	(282-583)	821	110	201/172	(92-278)	144
"0° - 30°S"									

[a] Singh et al. [1992b].

[b] Singh et al. [1994].

[c] Walega et al. [1992].

[d] H. B. Singh, private communication, 1995.

[e] H. B. Singh, private communication, 1995.

winter and early spring when there is little sunlight to support tropospheric PAN production north of 50°N, mixing ratios continue to increase. This suggests that the buildup of PAN may be the result of poleward and upward transport from the surface combustion emission regions farther south where sufficient sunlight, NO_x, and NMHC exist to produce PAN (this is explored in section 3.3).

3. While the SH also has its maximum PAN accumulation during the austral winter and spring, this maximum is located in the subtropical free troposphere and only minor poleward transport is noted during winter and spring. This implies the SH source regions are dominated by convective transport rapidly mixing PAN upward from continental surface production regions.

Figure 1 suggests that the distribution of PAN is related to the type of transport occurring in its formation regions as well as seasonal variations in tropospheric temperature. To examine this further, we present the geographical fields of PAN in Figures 2a and 2b, which display the 500-, 835-, and 990-mbar pressure levels for January and July, respectively.

In general, NO_x emissions appear to control the distribution of PAN at 990 mbar, with the highest levels confined to the continental source regions and lowest levels found over the oceans. In the NH winter, however, we find that away from continental source regions north of 30°N, PAN is uniformly spread with values in the 0.2 to 0.5 parts per billion by volume (ppbv) range. This is a result of the strong midlatitude winter circulation rapidly mixing PAN northward and eastward from

Table 2. Comparison of Model Simulation Wtih Observed Data Ranges

Region	Observations	Pressure	Range	Model Result		
				Mean/Med	50%	s.d.
Alert, Canada[a]	winter	sfc	[150 - 250]	372/352	(308-423)	88
82°N	spring		[250 - 500]	392/387	(367-409)	45
	summer		[< 50]	39/31	(15-63)	30
	fall		[75 - 100]	117/123	(58-165)	51
E. Pacific flight[b]	Feb.	315	[180 - 210]	166/152	(109-217)	77
40°N		500	[80 - 200]	261/243	(170-325)	117
E. Pacific flight[c]	Aug.	315	[20 - 50]	82/82	(54-107)	35
40°N		500	[10 - 50]	75/75	(54-95)	28
Colorado-[b]	July	315	[100 - 200]	71/71	(53-89)	27
Wyoming flight		500	[70 - 150]	89/83	(59-112)	44
E. Atlantic cruise[d]	Sept.-Oct.	sfc				
45°N - 40°N			[100 - 200]	82/28	(6-105)	129
40°N - 35°N			[5 - 25]	20/5	(2-15)	46
< 35°N			[~ 1]	2/1	(1-2)	4
E. Pacific cruise[b]	Nov.-Dec.	sfc				
(129°E)						
48°N - 25°N			[30 - 80]	136/93	(37-187)	135
25°N - 0°			[40 - 5]	14/10	(5-17)	16
0° - 48°S			[~ 5]	17/10	(2-23)	23

[a] Barrie and Bottenheim [1991].

[b] Singh et al. [1986].

[c] Singh et al. [1990b].

[d] Muller and Rudolph [1992].

the dominant combustion emission regions of the eastern United States, Europe, China, and Japan during the period of longest PAN lifetime. This is not seen in the SH winter. There, the combustion, biomass, and biogenic NO_x emission areas are mainly located in the tropics and subtropics, well equatorward of the midlatitude westerly winds and cyclonic disturbances. During the summer season of both hemispheres, PAN is confined to continental formation regions. Any boundary layer transport away from these areas leads to rapid PAN decay due to warmer temperatures.

At 835 mbar (~1.8 km) we observe further evidence of the different transport regimes affecting the NH and SH PAN formation regions. During the NH winter when essentially no convective transport is taking place north of 30°N, PAN is found to be well mixed due to strong transport associated with transient synoptic scale cyclones. As is shown in sections 3.4 and 4.3, these systems tend to occur on the order of 3 to 5 days. Downstream of their path, tracer transport is typically northeastward and upward where stronger westerly winds mix the tracer longitudinally, while a southeastward and downward advection occurs behind them. Even in the monthly mean, lifting due to these synoptic systems along predominant storm tracks produces PAN values greater than 0.5 ppbv over eastern North America, northeast of the major surface NO_x emission region farther south. This effect is also indicated over eastern Europe and northern Asia. An example of this

process is presented in section 3.4. In the SH winter at 835 mbar, however, areas of maximum PAN are confined to the subtropical continental NO_x source regions, indicating convective, not baroclinic, lifting and essentially no poleward transport. In the summer of both hemispheres, midlatitude storms are weak, and convective processes dominate.

In the cold midtroposphere at 500 mbar (~5.5 km), midlatitude temperatures support long PAN lifetimes of approximately 1 month in winter and 7-10 days in summer. Even in the subtropics, lifetimes are of the order of 5 days. Therefore any PAN transported to this altitude will tend to accumulate, albeit more so in winter. This can be seen in the NH winter where midlatitude storms described above have transported PAN aloft and strong west to east winds associated with the upper tropospheric jet stream have zonally distributed PAN values greater than 0.2 ppbv. During summer, PAN mixing ratios north of 40°N decrease to the 0.1 to 0.2 ppbv range due to the absence of baroclinic lifting and somewhat shorter lifetimes. The SH winter subtropics produce a belt of PAN greater than 0.05 ppbv with embedded areas greater than 0.1 ppbv over continental regions, extending from South America across Africa to Australia. This feature can also be seen in January, although values are slightly smaller. This band of relatively high PAN mixing ratio is the result of colder 500 mbar temperatures and stronger winds which advect PAN west to east after it has been vertically lifted by convective processes.

JANUARY PAN (ppbv)

APRIL PAN

JULY PAN

OCTOBER PAN
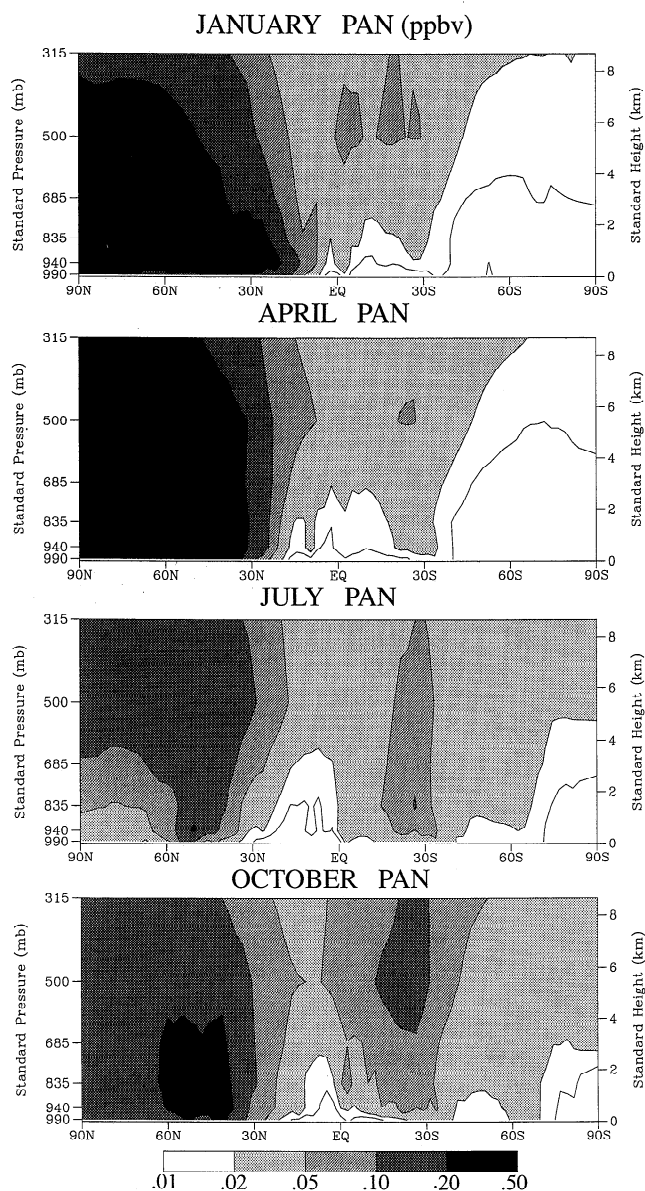
Figure 1. Simulated zonal mean PAN mixing ratios (parts per billion by volume (ppbv)) for the months of January, April, July, and October.

3.3. PAN Chemistry and Implied Transport

Our examination of the diverse global distribution of PAN implies a complex interaction, both direct and indirect, among the location and magnitude of NO_x emissions, tropospheric temperature, photochemistry, and transport of PAN. To gain farther insight into this complicated interdependency, keeping in mind that both NO_x emissions and PAN occur predominantly in the NH, we first present the monthly global tropospheric integrals of "NO_x emissions," "PAN," "PAN production," and "PAN loss" (Figure 3a) and "PAN production minus loss" (Figure3b). As one would expect, NO_x emissions, PAN production, and PAN loss are basically in phase with maxima during the NH summer (July-September) when combustion NO_x emissions are enhanced by biomass and biogenic sources. The integral of PAN itself, however, is out of phase, with its maxima occurring during the NH early spring when tropospheric temperatures are lowest, minimizing PAN

loss. What is noteworthy is that while the PAN production and loss are large terms (~0.05 Tg N d^{-1}), the daily net chemistry is very small (~ 2 orders of magnitude less). Clearly, on a global scale the small difference between the large formation and the thermal decomposition of PAN produces a delicate balance and the relationship between the global tropospheric levels of PAN and the PAN chemistry is relatively subtle.

Additional information regarding this balance as well as a preliminary clue to the role of transport in the accumulation of PAN are provided in Figures 4a, 4b, and 4c which display the latitudinal structure in the monthly vertical integrals (315-990 mbar) of PAN, NO_x emissions from all six sources, and the zonally averaged monthly net PAN production at 990 mbar, where fossil fuel combustion and biomass burning emission regions produce a maximum in PAN formation.

We first consider the SH, which appears to be straightforward. The NO_x emissions, the net PAN production, and PAN itself all show a maximum at the same general subtropical latitude during winter and early spring, when the primary NO_x source, biomass burning, is a maximum and tropospheric temperatures are a minimum. Here, in the subtropics, solar insolation is still strong enough for the photochemical production of the PAN, while cooler seasonal temperatures allow longer

JANUARY
PAN 500mb

PAN 835mb

PAN 990mb
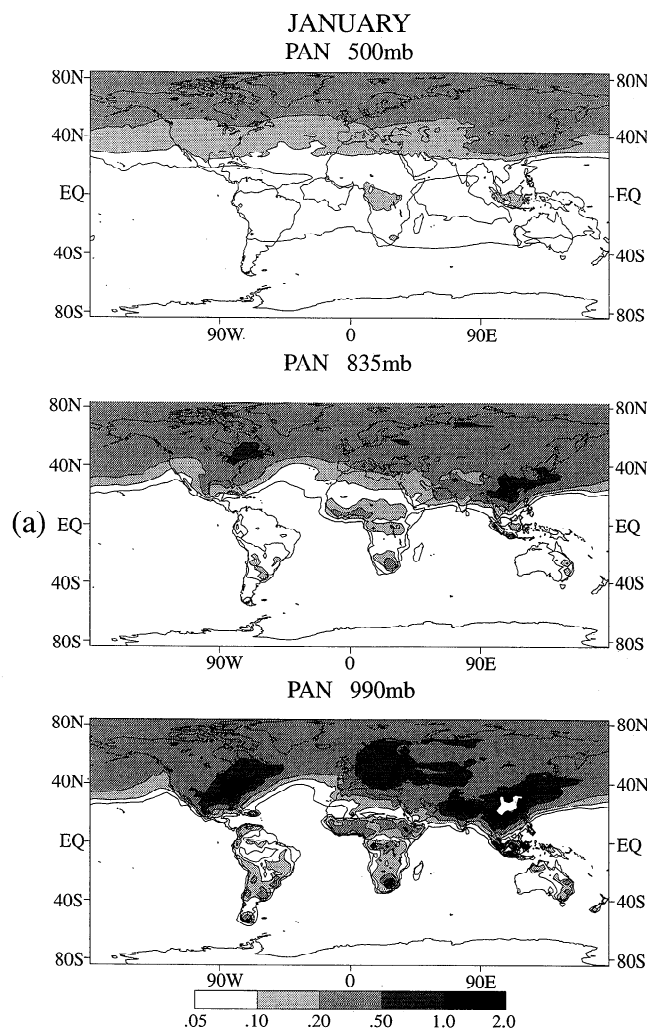
Figure 2a. Simulated January mean PAN mixing ratios (ppbv) at 500, 835, and 990 mbar. Areas of white within black shading indicate values between 2 and 5 ppbv.

JULY
PAN 500mb

PAN 835mb

PAN 990mb

.05 .10 .20 .50 1.0 2.0
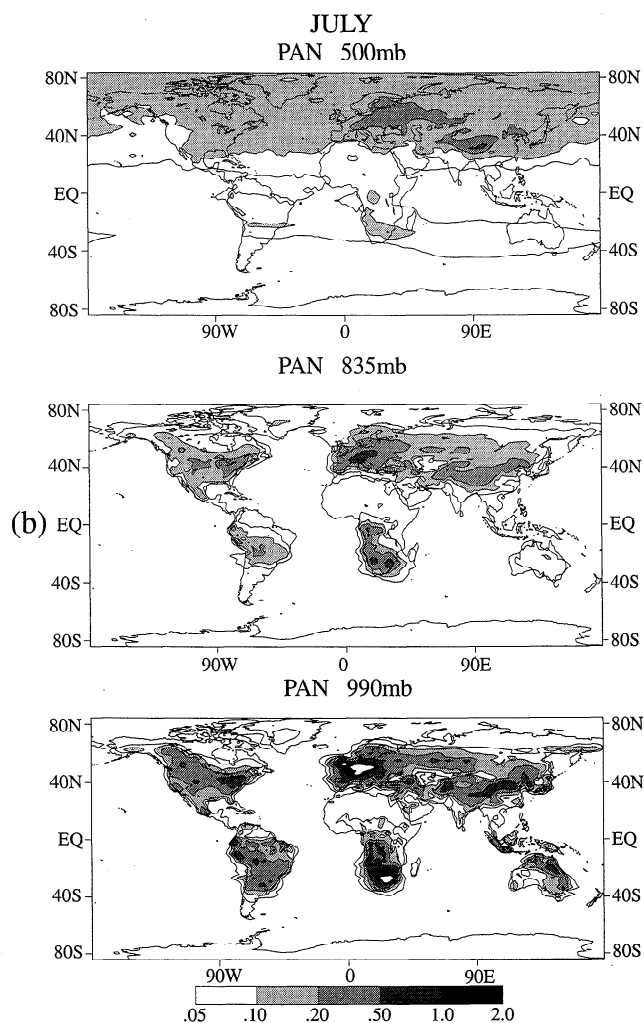
Figure 2b. Simulated July mean PAN mixing ratios (ppbv) at 500, 835, and 990 mbar. Areas of white within black shading indicate values between 2 and 5 ppbv.

PAN lifetimes. The PAN produced is then rapidly mixed upward by moist and dry convection, as suggested in Figures 1 and 2b.

However, unlike the SH, the processes in the NH are more complex and can be summarized as follows:

1. As seen in Figure 4b, the dominant NO_x sources are located in midlatitudes between 30°N and 55°N, associated with the major population centers of the United States, Asia, and Europe. These emissions are dominated by fossil fuel combustion, which is constant throughout the year, and summertime biogenic processes.

2. During winter and early spring when PAN lifetimes are long, transport is dominated by midlatitude synoptic scale storm systems.

3. Solar insolation, strong enough to allow net PAN production, progresses south to north with time across the NO_x emission regions.

Although significant NO_x emissions are available throughout the year, the above conditions produce a seasonal and spatial structure in the net PAN production, which is seen zonally in Figure 4c. From November to March, enough solar insolation occurs over the eastern United States and Asia south of 45°N to produce dominant PAN production. As spring ar-

rives, Europe begins to play a role and, by summer, is a major contributor of net PAN production. In contrast to the narrow bands of NO_x emissions and net PAN production, synoptic scale transport advects PAN away from its net production regions producing a broad area between 30°N and 70°N. This is the direct result of northward and upward transport from net PAN production regions along the east coasts of the United States and Asia into the cold free troposphere by strong midlatitude storms which are most prevalent from late fall through spring. In Europe these storms are sometimes deflected north by upper atmosphere blocking patterns, transporting pollution directly into the Arctic [*Iverson*, 1993]. During summer, even though the formation rate reaches a maximum, meteorological transport substantially weakens and the entire NH troposphere warms, reducing PAN by thermal decay.

3.4. Midlatitude Synoptic PAN Transport

As an example of the synoptic transport discussed above, we present a simulated midlatitude surface cyclone and its associated cold front which occurred over eastern North America during the integration of our model. On February 18, as seen in Figure 5a, a cold front (thick line) extends from a deep low over Hudson Bay south and west across the western Great Lakes into Texas and proceeds to move to the U.S. East Coast by February 20 (Figure 5b). To examine the effect of this system on the transport of PAN from its eastern U.S. production region, it would be useful to have a set of conservative physical surfaces in the atmosphere. It then would be possible to measure air motion and its transport in three dimensions by an analysis of this surface at successive times. Since atmospheric processes in the free troposphere tend to be dry adiabatic in the short term (no diabatic heating
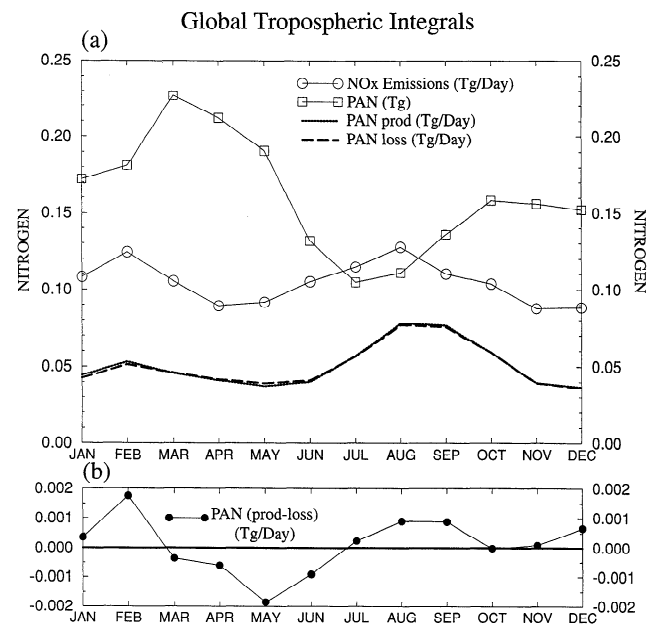
Figure 3. Simulated monthly global tropospheric integrals (315-990 mbar, from 90°S to 90°N). (a) NO_x emissions from all six sources, PAN, PAN production, and PAN loss. PAN values are computed at the first of each month in units of teragrams (Tg) of nitrogen. The other integrals are in units of Tg nitrogen per day. (b) PAN "production minus loss" in units of Tg nitrogen per day (note the change in the scale of the y axis).

PAN

(a)

NOx EMISSIONS

(b)

NET PAN PRODUCTION

(c)
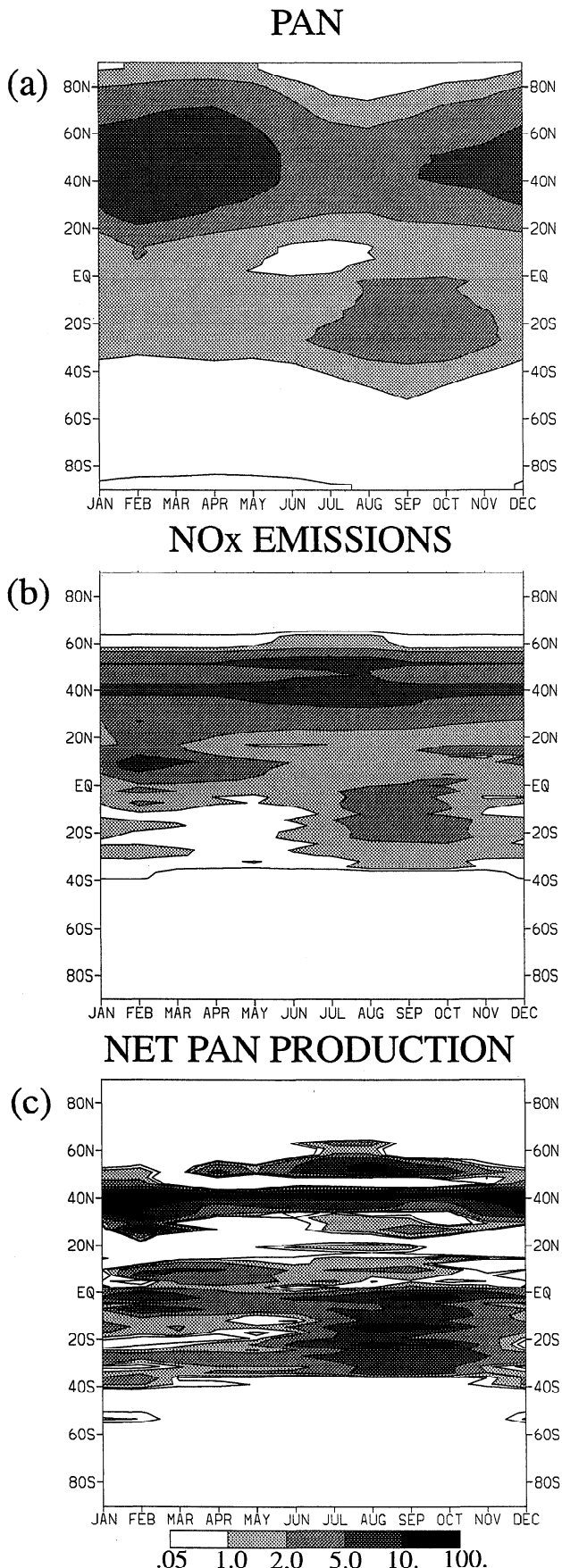
or cooling due to precipitation or radiation), a given isentropic (constant potential temperature) surface is conserved over time. In view of this, we will examine the PAN mixing ratio field as it evolves on an isentropic surface. Its constant potential temperature θ is defined as

$$\theta = T \left[\frac{1000}{P} \right]^{\kappa} \qquad (1)$$

and T is temperature, P is pressure, $\kappa = R_d/C_p$, R_d is the gas constant for dry air, and C_p is the specific heat of dry air at constant pressure. Therefore the height of an isentropic surface typically increases poleward with colder temperatures, providing a unique quasi three-dimensional view of the tracer field.

Figures 5c, 5d, and 5e display PAN mixing ratios on the 285° isentropic surface during model dates February 18, 20, and 22. This surface was chosen because it intersects the ABL over the eastern U. S. PAN production region and rises to approximately 500 mbar at high latitudes (as indicated by the superimposed lines of constant pressure). On February 18, mixing ratios greater than 2 ppbv exist in the ABL over the eastern United States. As the model cold front approaches from the west, its dynamics provide a southwest to northeast flow of air in a region of rising motion similar to observed cold fronts [*Carlson*, 1980]. By February 20 the area of large PAN values has been swept northeast and upward, resulting in PAN mixing ratios greater than 0.5 ppbv being found from the U. S. East Coast into the free troposphere over eastern Canada. Two days later, the original storm has dissipated (not shown), however, in its wake areas of significant PAN mixing ratios greater than 0.5 ppbv have been transported irreversibly into the midtroposphere over northern Canada and Greenland and above 600 mbar, background values are now greater than 0.2 ppbv (Figure 5e). At the same time, over the southeastern United States where the 285° isentropic surface now intersects the ABL, PAN values have begun to increase and are available again for transport by the next midlatitude eastward moving storm system.
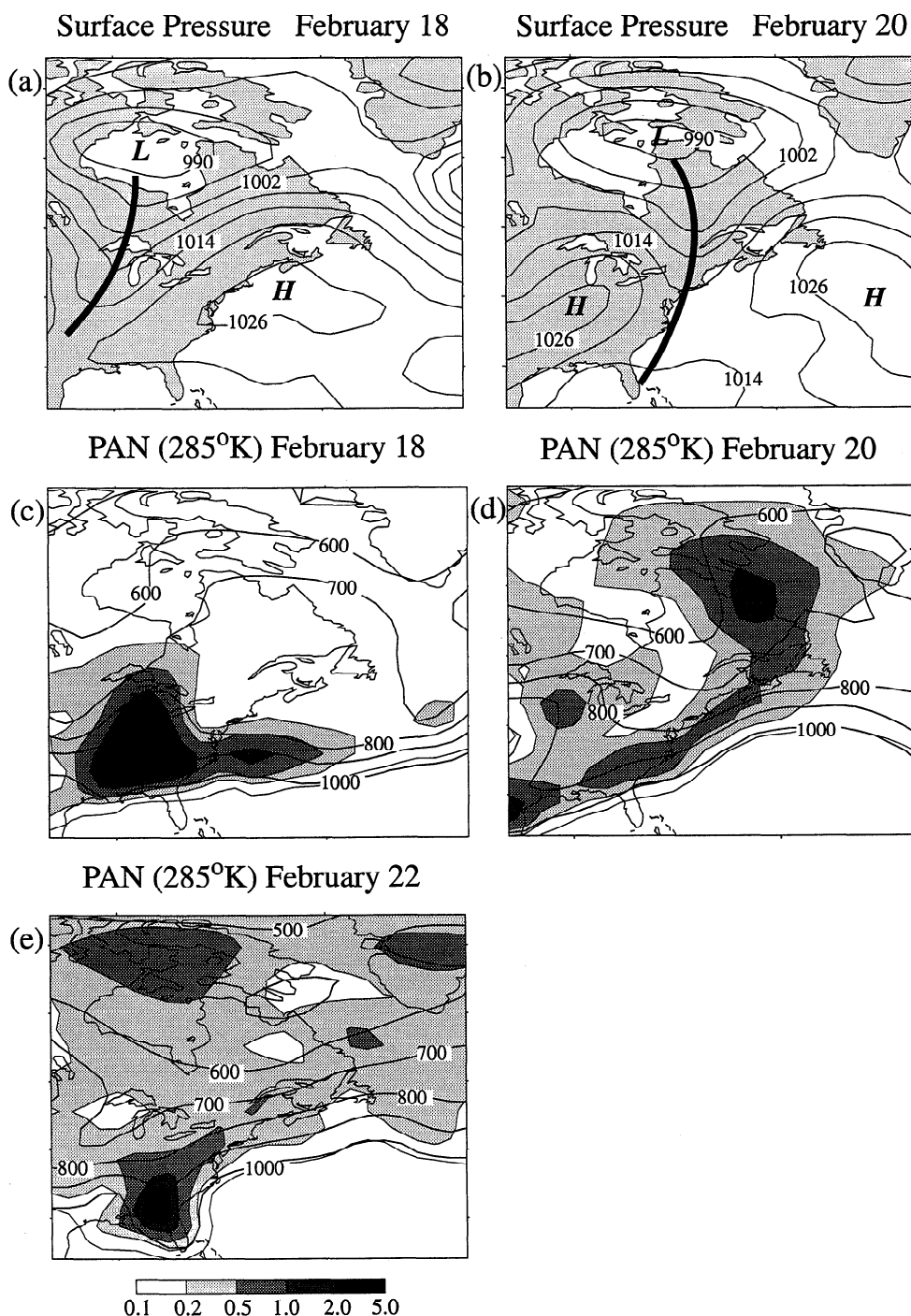
It should also be noted that behind synoptic systems, tropospheric air is transported from the colder north to the warmer south along isentropic surfaces and from equation (1) we see that this implies sinking motion. As is shown in section 4.3, this process is important in tapping the midtroposphere reservoir of PAN and transporting it southward and downward to the warm ABL, potentially producing a thermal release of NO_x.

4. PAN's Role in Tropospheric NO_x Distribution

In section 3.2 it was shown that PAN mixing ratios, particularly in the colder regions of the troposphere, can be quite high and, as a first impression, imply significant NO_x storage in the form of PAN. However, a reexamination of Figure 3a, where we presented the global tropospheric integrals for

Figure 4. Simulated zonal mean vertical integrals (315-990 mbar) versus time of (a) PAN, (b) NO_x emissions from all six sources, and (c) net PAN production (PAN production minus PAN loss > 0) at 990 mbar. Units are grams of nitrogen scaled by 1×10^9 for PAN and NO_x emissions and 1×10^5 for net PAN production.

Surface Pressure   February 18   Surface Pressure   February 20

PAN (285°K) February 18   PAN (285°K) February 20

PAN (285°K) February 22

0.1   0.2   0.5   1.0   2.0   5.0

Figure 5. Surface pressure (mbar) with a 6 mbar interval (thick dark line indicates the cold front) at (a) model date February 18 and (b) model date February 20 and PAN mixing ratios (ppbv) on the 285°K isentropic surface (denoted by shading) at (c) model date February 18, (d) model date February 20, and (e) model date February 22. The contours represent lines of constant pressure (mbar) interpolated to the 285°K isentropic surface.

monthly mean PAN and daily NO_x emissions in terms of mass of nitrogen, shows that even at its maximum the total mass of nitrogen stored as PAN is only of the order of 2 days of global NO_x emissions or about 9% of tropospheric NO_y. In view of this, we would expect little impact by PAN on the global tropospheric NO_x levels. However, this does not exclude a regional or local influence.

4.1. PAN Chemistry Versus No-PAN Chemistry "Global Tropospheric Influence On NO_x"

Similar to *Kasibhatla et al.* [1993], we explicitly test the impact of PAN chemistry on the distribution of tropospheric NO_x by performing the same numerical integration outlined in section 2, but with only two species (NO_x and HNO_3) being transported and all chemical reaction rates involving the for-

Table 3. January NO_x and PAN Global Tropospheric Balances (Tg N / day)

NO_x Formation	NO_x Loss
NO_x emissions = 0.1016	[NO_x to HNO3] = 0.0971
[PANtemp to NO_x] = 0.0414	[NO_x to PAN] = 0.0444
[PANoh to NO_x] = 0.0007	NO_x dry deposition = 0.0092
[HNO$_3$ to NO_x] = 0.0072	
Total formation = 0.1509	total loss = 0.1507
[NO_x formation - NO_x loss] = +0.0002	

PAN Formation	PAN Loss
[NO_x to PAN] = 0.0444	[PANtemp to NO_x] = 0.0414
	[PANoh to NO_x] = 0.0007
	PAN dry deposition = 0.0020
Total formation = 0.0444	total loss = 0.0441
[PAN formation - PAN loss] = +0.0003	

mation and destruction of PAN removed. As expected, an examination of the monthly global tropospheric integrals of NO_x (not shown) for both the "PAN" and the "no-PAN" integrations showed that within 4% the magnitude and seasonal variations are the same. The explanation for the similarity in the PAN and no-PAN integrals is found in Table 3, where we present the simulated January global tropospheric balances (241 mbar to the surface, from 90°S to 90°N) for both the NO_x and the PAN photochemical cycles. The largest NO_x loss path is its conversion to HNO3, which is quickly removed from the system through wet and dry deposition, followed by conversion to PAN (~ a factor of 2 less) and the relatively small NO_x dry deposition. The significant NO_x to PAN reaction path at first infers a possible large storage of nitrogen in the form of PAN, until we notice that this loss is nearly balanced by PAN's thermal decomposition back to NO_x plus the minor reaction of PAN with OH. As discussed previously and shown here, the PAN-NO_x cycling is nearly in balance leading to a slow January tropospheric buildup of PAN and a subsequent minor sequestering of potential NO_x. The NO_x to HNO3 loss path, however, is more than 2 orders of magnitude greater and completely dominates the removal of NO_x from the global tropospheric system.
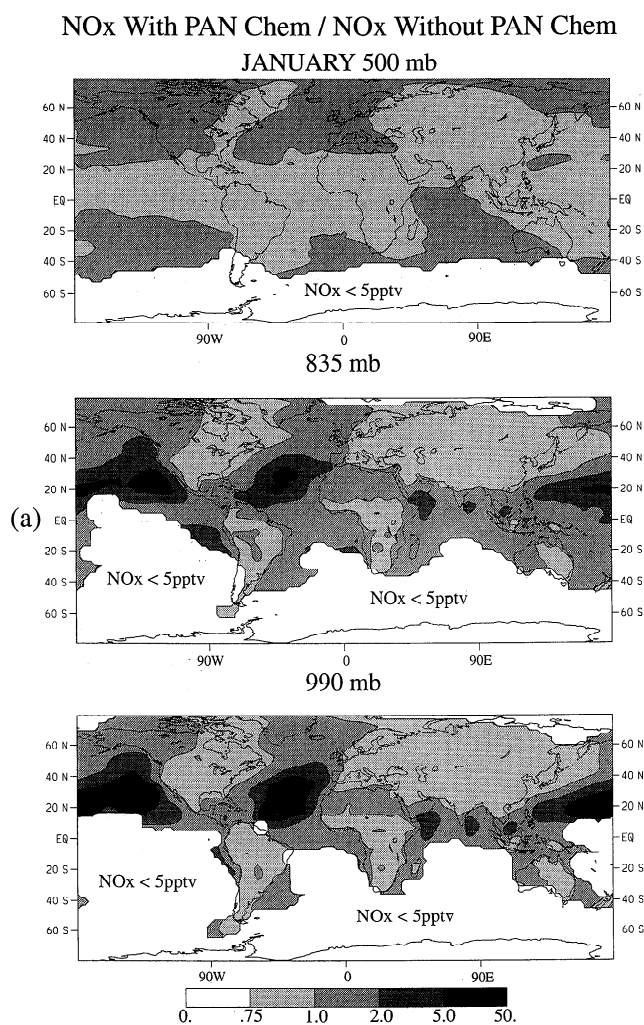
While PAN chemistry has little affect on the global tropospheric integral of NO_x, an analysis of its geographical influence reveals that it does significantly change the NO_x global distribution. To examine PAN's impact, we display in Figures 6a and 6b, the January and July ratio of NO_x with PAN chemistry, to NO_x without PAN chemistry in the ABL (990 mbar), the lower troposphere (835 mbar), and the midtroposphere (500 mbar) for NO_x values greater than 5 pptv.

Throughout the year in the NH lower troposphere and the ABL the addition of PAN chemistry generally increases the NO_x levels over much of the oceans and slightly decreases NO_x levels over the continental source regions (less than 10%). The largest enhancement of NO_x, more than a factor of

5, is found in the remote winter subtropics, while in the summer, a factor of 2 increase occurs in oceanic midlatitudes.This is also true in the SH. However, except for the winter subtropics, mixing ratios are small, having values less than 5 pptv.

In contrast to the lower troposphere, the influence of PAN chemistry at 500 mbar is small (less than 10%). At this level and above, cold global temperatures throughout the year produce long PAN lifetimes and preclude any significant thermal decomposition to NO_x. Also, the land-sea contrast depicting a reduction of NO_x over the continents and an increase over the oceans seen in the lower regions of the troposphere is less distinct, however, an area of reduced NO_x appears along the east coast of North America. In the tropics, PAN chemistry produces a general zonal region of reduced NO_x.

These general results can be qualitatively explained as follows, with the inclusion of PAN: (1) In the oceanic remote lower troposphere, NO_x increases significantly, apparently due to the thermal release of NO_x from PAN after transport from colder to warmer regimes. It is this process and its potential affect on ozone production that will be explored in the following sections. (2) Over NO_x emission areas in the continental source regions the amount of NO_x present decreases, simply as a result of it being converted to PAN. (3) The reduction of NO_x observed over the midlatitude continents at 850 mbar during winter is a result of upward transport of decreased surface values described in result 2 above. This is especially evident along the East Coast storm track of North America where synoptic scale weather systems described in section 3.3 (see Figure 5) vertically transport reduced NO_x values north and east from surface source regions. The remnants of this process can even be observed at 500 mbar. (4) In the upper troposphere, PAN's influence on NO_x is small due to long lifetimes associated with cold temperatures. (5) In the continental tropics the reduced surface NO_x (from result 2 above) is vertically transported by convection where stronger

NOx With PAN Chem / NOx Without PAN Chem
JANUARY 500 mb

NOx With PAN Chem / NOx Without PAN Chem
JULY 500 mb

Figure 6a. January ratio of NO_x (with PAN chemistry) to NO_x (without PAN chemistry) at 500, 835, and 990 mbar. Ratios were not plotted for largest local NO_x values less than 5 pptv.
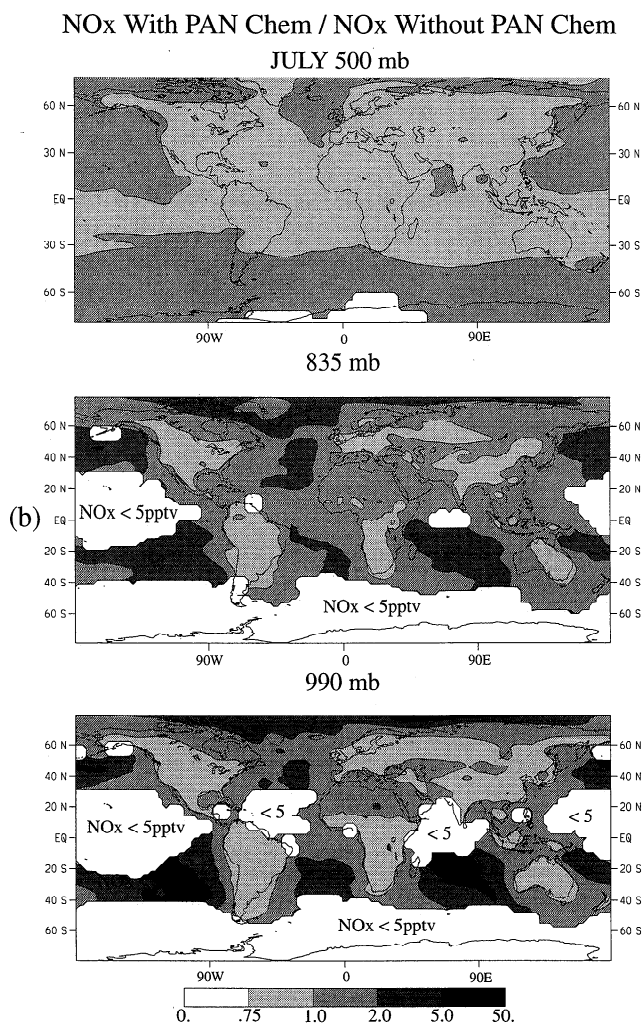
Figure 6b. July ratio of NO_x (with PAN chemistry) to NO_x (without PAN chemistry) at 500, 835, and 990 mbar. Ratios were not plotted for largest local NO_x values less than 5 pptv.

westerly winds produce a general zonal distribution in the middle and upper troposphere.

It is interesting to note that the redistribution of NO_x resulting from the inclusion of PAN also has a direct influence on the simulated ABL HNO_3 and its wet deposition. Previously, an examination of the impact of stratospheric NO_x on the tropospheric NO_y levels [*Kasibhatla et al.*, 1991] showed that lower-tropospheric HNO_3 mixing ratios were enhanced 10-50% when PAN chemistry was included. Also, it has recently been speculated that PAN chemistry is needed to produce the observed values of HNO_3 and nitrate deposition in remote regions [*Roelofs and Lelieveld*, 1995].

An examination of our results reveals that the ratio of wet deposition with PAN chemistry to wet deposition without PAN chemistry (not shown) depicts increases in HNO_3 deposition over remote oceanic areas similar to the increases in NO_x seen at 990 mbar. This suggests that most of the wet deposition found in these regions results from locally produced HNO_3 rather than direct transport from continental NO_x source regions.

4.2. Monthly PAN Versus No-PAN Chemistry "Remote Regional Influence"

PAN's role in the redistribution of NO_x may have an additional impact by potentially altering regions of ozone production and destruction. A number of theoretical studies of the NO_x control over ozone's net chemical tendency in the troposphere have inferred that the switch from ozone production to ozone destruction varies widely for normal tropospheric ozone values due to its sensitivity to the actual ozone mixing ratio, the amount and nature of NMHC present, the atmospheric temperature, and the water vapor mixing ratio [e.g. *Levy et al.*, 1985; *Chameides et. al.* 1987; *Lin et al.*, 1988; *Carroll et al.*, 1990; *Ridley et al.*, 1992; *Liu et al.*, 1992; A. Klonecki and H. Levy II (manuscript in preparation, 1996)]. Therefore it is not possible to state that a specific NO_x value represents the balance point between ozone production and destruction. However, it is generally safe to assume that away from the polluted boundary layer, air with NO_x less than 20 pptv is photochemically destroying ozone and air with NO_x greater than 75 pptv is photochemically producing it.

In our model simulation the small decrease of NO_x over continental emission areas when PAN chemistry is included has little impact on regional tropospheric ozone, since NO_x levels are already quite high during the seasons of ozone production. However, in the ABL over remote oceans, where NO_x values are near the balance point between ozone production and destruction, the enhancement resulting from PAN chemistry may be significant. Before examining these regions in more detail, one should keep in mind the complex interactions between seasonal variations in chemistry due to changes in solar angle and temperature, and shifts in the transport meteorology.

We first present the local seasonal structure of NO_x with and without PAN chemistry at 990 mbar in the NH. Although PAN chemistry in the SH winter can increase the NO_x mixing ratios up to a factor of 5 in the ABL, the simulated NO_x values themselves are too small to allow ozone production. In Figure 7, three monthly mean time series are shown at selected model grid boxes: the North Atlantic (55°N,35°W), the central North Atlantic (35°N,45°W), and the subtropical eastern North Pacific (30°N,155°W). In general, we note that the largest NO_x mixing ratios occur from late fall to early spring with the greatest contribution from PAN chemistry during early spring, while warm temperatures and the strong solar insolation of summer produce low NO_x values due to rapid thermal decomposition of PAN and subsequent quick conversion of NO_x to HNO_3.

At 55°N,35°W in the North Atlantic during winter (December through February) the longer NO_x lifetime leads to mixing ratios in the 120 to 140 pptv range with a significant decrease during February, while contributions from PAN are small (less than 25 pptv) due to cold temperatures. The large February decrease is a result of reduced transport from the NO_x emission region of eastern North America due to meteorological variability. As the solar insolation continues to increase during spring, NO_x values begin to decrease, while concurrently, PAN's thermal decomposition resulting from warmer temperatures leads to a significant enhancement of NO_x during April and May (40-55 pptv). This result tends to support the suggestion by *Penkett and Brice* [1986] that the spring maximum of PAN seen in clean air at high latitudes could contribute to the observed maximum in tropospheric ozone. However, even though PAN's role is important, it is noteworthy that the NO_x late winter-early spring mixing ratios obtained without PAN chemistry are probably large enough to support ozone production.

Examining grid boxes farther south over the truly remote areas of the North Atlantic and North Pacific Oceans, a somewhat different story unfolds. Here, we observe that the maximum NO_x increase resulting from PAN is found earlier in the year during March as a result of a warmer ABL. The increase in NO_x due to PAN chemistry is somewhat larger than the increase in the 55°N,35°W grid box, producing NO_x values near the ozone production range. Unlike the more northern latitudes however, monthly mean NO_x values without PAN chemistry remain too low to possibly generate ozone. Also, the simulated NO_x in the remote eastern Pacific Ocean throughout the entire year is solely the result of PAN chemistry.

To gain better insight into the vertical structure of PAN's influence on NO_x, we display profiles of simulated NO_x above these same grid boxes during the month of March when PAN's impact is at or near a surface maximum (Figure 8). At

higher latitudes (55°N,35°W), PAN chemistry affects NO_x only in the bottom two model levels where the ABL is modified by the relatively warm ocean temperature, while over warmer remote regions farther south, a greater depth of the troposphere is affected. Also, at 35°N and 30°N the NO_x profile actually reverses from one decreasing with height to one increasing with height when PAN chemistry is not included. Note that in the cold upper troposphere the addition of PAN chemistry has little affect on NO_x.
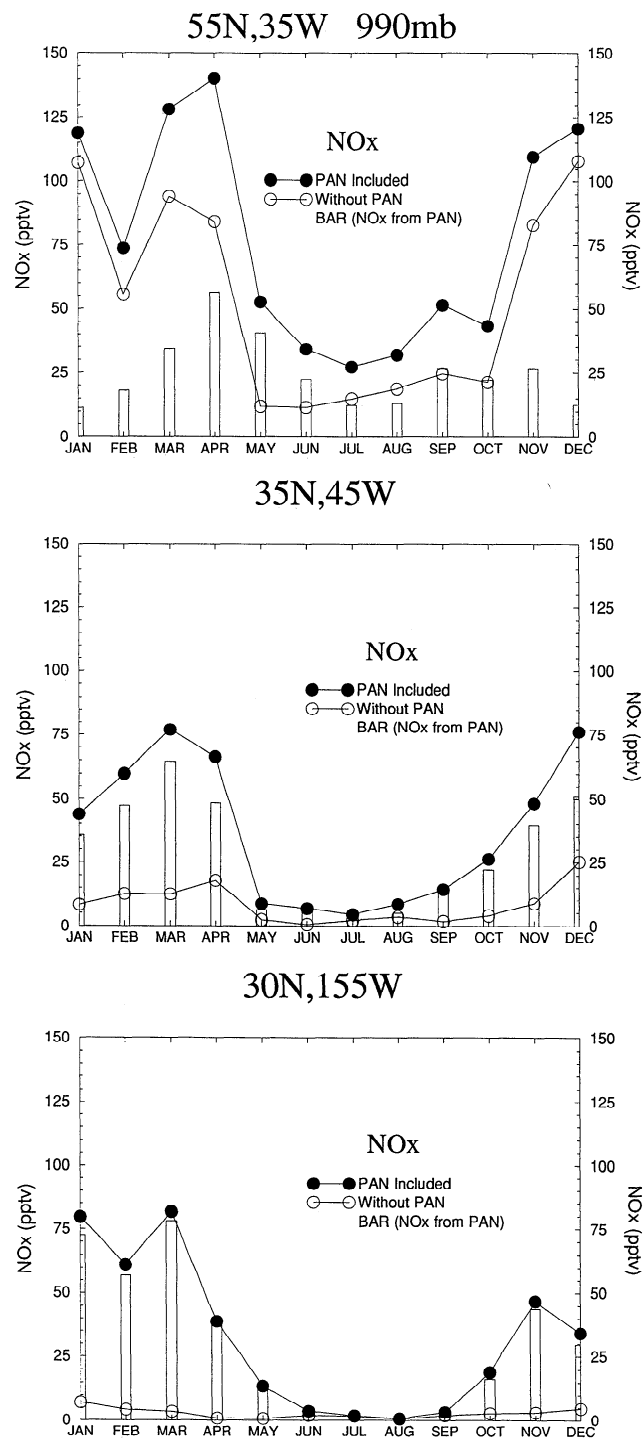
**Figure 7.** Monthly mean time series of NO_x (pptv) at 990 mbar with and without PAN chemistry for the selected model grid boxes (55°N,35°W), (35°N,45°W), and (30°N,155°W). The bars denote the NO_x produced by PAN chemistry.

MARCH

55N,35W

35N,45W

30N,155W

Mixing Ratio (pptv)
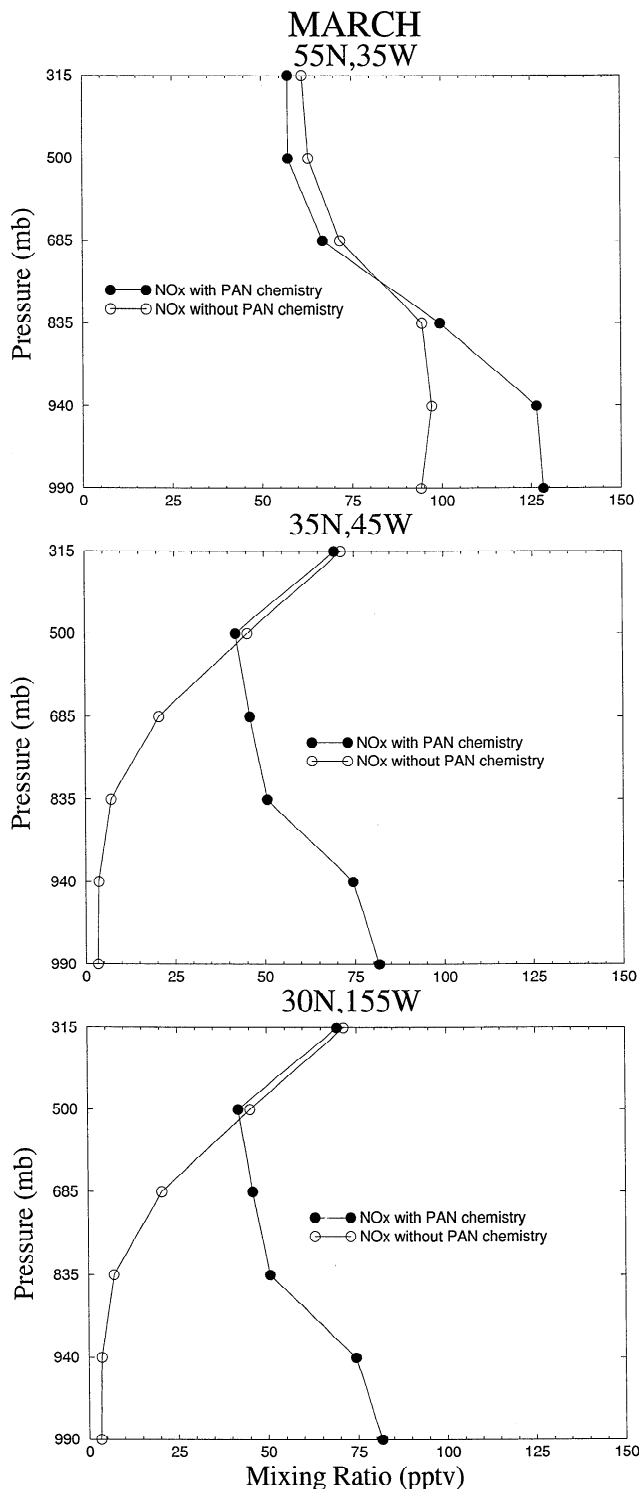
Figure 8. March vertical profiles of NO_x (pptv) with and without PAN chemistry for the selected model grid boxes (55°N,35°W), (35°N,45°W) and (30°N,155°W).

4.3. Synoptic Fluctuations and Local Transport Events

For a more detailed and quantitative analysis of the role PAN and its transport plays in NO_x levels far from source regions, it would be helpful to know explicitly the contributions to a remote local NO_x mixing ratio from unconverted NO_x transported from emission regions and NO_x resulting from
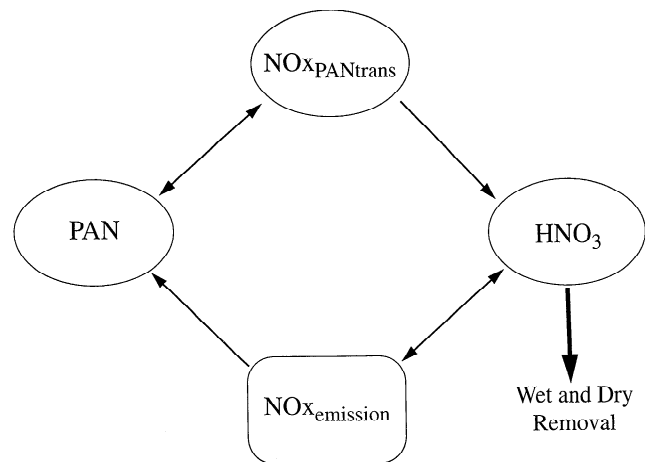
Figure 9. Diagram of the four tracer integration where NO_x was segregated into two separate tracers: $NOx_{emission}$ and $NOx_{PANtrans}$.

PAN decomposition. To accomplish this, we devised a third experiment employing four tracers. In addition to HNO_3 and PAN, NO_x was segregated into two separate tracers: NO_x that is emitted from any of the six sources and never converted into PAN ($NOx_{emission}$) and NO_x that is formed from PAN decomposition after the PAN is transported away from the NO_x source regions ($NOx_{PANtrans}$). In the context of ($NOx_{PANtrans}$) the "NO_x source region" is defined as any surface grid box containing NO_x emission, plus a buffer zone of one grid box in both the horizontal and the vertical to account for strong local diffusion of PAN and NO_x. In this experimental design, as shown in Figure 9, the two NO_x tracers can form PAN; however, PAN can only form $NOx_{PANtrans}$. In addition, they both produce HNO_3, but HNO_3 can only form $NOx_{emission}$. Also, unlike the "no-PAN" experiment discussed in section 4.1 which produces enhanced NO_x transport from source regions due to a lack of PAN formation, $NOx_{emission}$ provides an accurate measure of unconverted NO_x in remote areas.

By separating NO_x into two classes, we can explicitly detect the NO_x in remote regions that traveled from the source region as PAN. However, there is an inherent drawback in that the role of PAN formation in the remote troposphere, as speculated by *Singh and Hanst* [1981], is not adequately quantified. To obtain an estimate of the relative contribution of PAN formed from background NO_x and hydrocarbons versus PAN production in polluted areas available for subsequent transport, we calculated monthly integrals of net PAN production (formation - loss > 0), where the polluted region was defined as the lower two model levels over combustion source grid boxes. The results showed that during the year, 90 to 95% of the net PAN production occurred in polluted areas, emphasizing the role of transport in the global distribution of PAN, rather than in situ production. Utilizing the above experimental design in concert with time series of model data generated every six hours and trajectory analysis of specific events, the nature of the transport mechanisms can be examined.

ABL time series at two remote sites examined earlier, the northern Atlantic Ocean (55°N,35°W) and the subtropical eastern Pacific Ocean (30°N,155°W), are presented in Figures 10a and 10b and 11a and 11b for the period January through May. Although we chose only two grid boxes for display, they

NOx from Emissions (55N,35W) 990mb

NOx from PAN Transport (55N,35W) 990mb
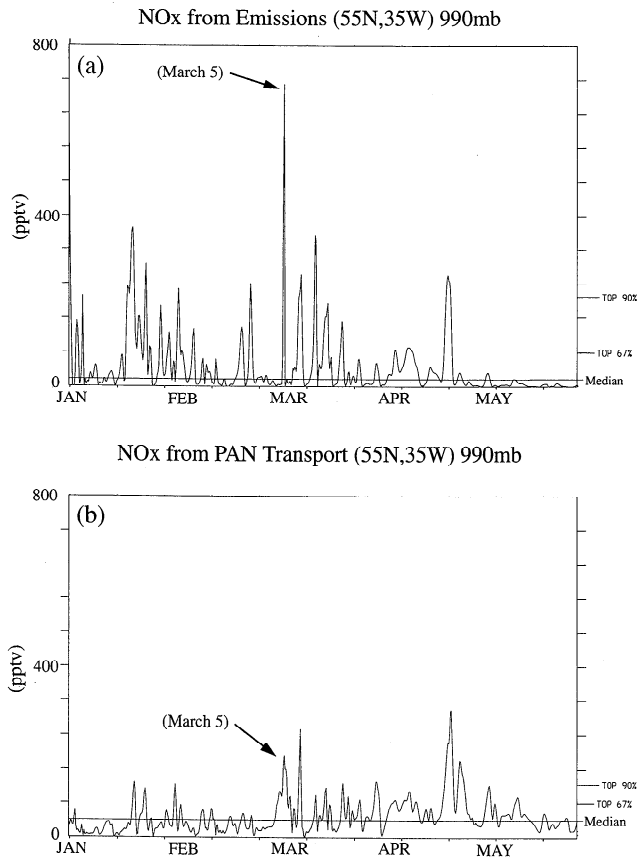
Figure 10. The (55°N,35°W) 990-mbar time series plot (every six hours) January 1 through May 31 for (a) $NOx_{cmissions}$ and (b) $NOx_{PANtrans}$. The arrows denote the NO_x episode chosen for trajectory analysis as depicted in Figure 12.

are representative of these general regions. We should first consider the general nature of the time series: (1) They are highly variable with NO_x ranging from a high near 700 pptv to a low of only a few parts per trillion by volume. (2) The fluctuations are synoptic in timescale with the NO_x peaks occurring every 3-10 days and lasting only 1 to 2 days, while their magnitude decreases rapidly in late spring as extratropical storm intensity wanes. (3) All tracers are highly correlated, indicating their respective peaks are a result of similar transport events.

Clearly, NO_x levels range quite rapidly between ozone production and ozone destruction. In fact, the actual seasonal mean for NO_x occurs infrequently so that low monthly mean mixing ratios of NO_x may still support periods of ozone production.

In the North Atlantic, as seen in Figures 10a and 10b, winter events associated with low solar insolation and cold temperatures are dominated by $NOx_{emission}$ being transported directly from the relatively close emission regions of North America and Europe, with mixing ratios greater than 200 pptv common. From late winter through spring, NO_x to HNO_3 conversion rates increase, decreasing $NOx_{emission}$, while warming allows $NOx_{PANtrans}$ to play a significant role. Examining the truly remote eastern North Pacific (30°N,155°W) time series shown in Figures 11a and 11b, we observe a reversal of the roles played by $NOx_{emission}$ and $NOx_{PANtrans}$, as compared with the North Atlantic. In this region, essentially all the NO_x results

from $NOx_{PANtrans}$, while the maximum $NOx_{emission}$ for the entire 5-month period (not shown) is only 8 pptv. It is interesting to note the strong correlation between the large PAN events and the $NOx_{PANtrans}$ events. These episodes of high PAN mixing ratios seem to imply strong sinking motions, since tropospheric flow is generally west to east in midlatitudes and any PAN transported in the ABL from the distant Asian source areas would thermally decompose to $NOx_{PANtrans}$ and then convert to HNO_3 before reaching the eastern Pacific. The only way PAN could survive the relatively long trip is to first be lifted to the cold midtroposphere, advected across the Pacific, and then sink southward.

The diverse types of transport suggested above, which take place over the North Atlantic and the eastern Pacific, can be readily seen when we examine the three-dimensional model trajectories associated with large NO_x events. Unlike isentropic trajectories, which have inherent problems due to lack of data and diabatic effects, model three-dimensional trajectories have no spatial or temporal voids and the vertical velocity is known exactly, leading to consistent trajectory calculations [*Moxim*, 1990]. By integrating these trajectories backward in time from any particular episode, one can analyze the nature and origin of the Lagrangian transport.

As denoted by the arrows in Figures 10 and 11, we chose a significant event from both the North Atlantic (55°N,35°W), where $NOx_{emission}$ and $NOx_{PANtrans}$ reached values of 710 and 192 pptv, respectively, and the eastern Pacific (30°N,155°W), where $NOx_{PANtrans}$ dominated with a mixing ratio of 172 pptv

NOx from Transported PAN (30N,155W) 990mb
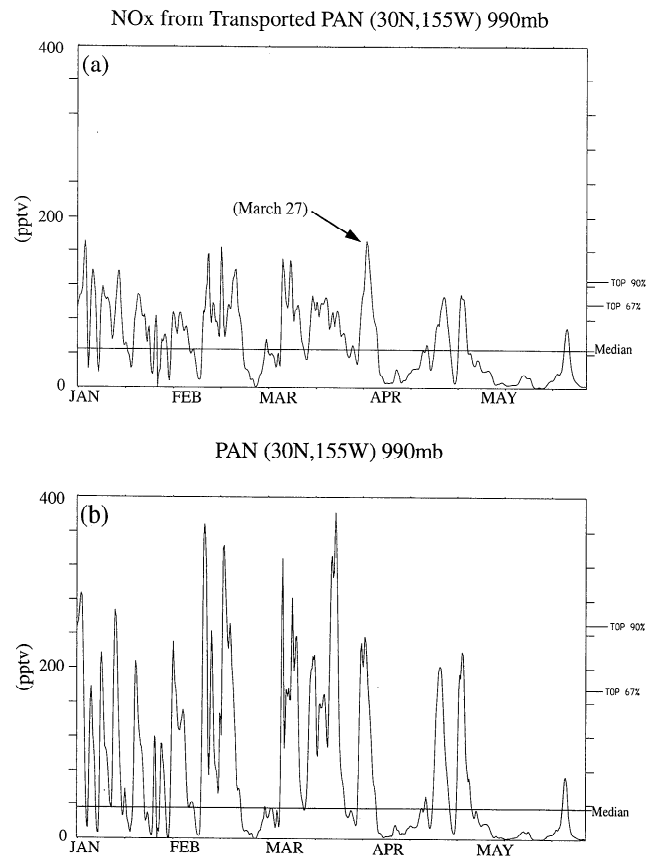
PAN (30N,155W) 990mb

Figure 11. The (30°N,155°W) 990-mbar time series plot (every six hours) January 1 through May 31 for (a) $NOx_{PANtrans}$ and (b) PAN. The arrow denotes the NO_x episode chosen for trajectory analysis as depicted in Figure 13a.
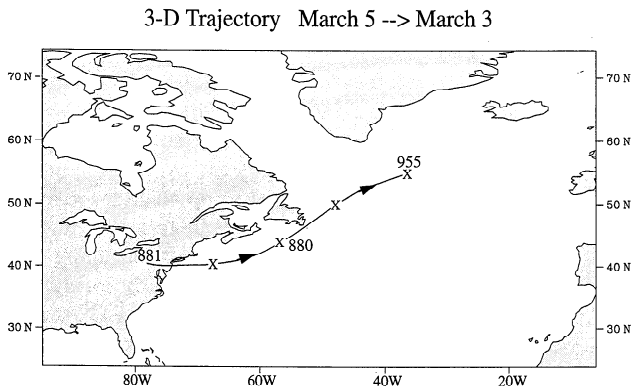
Figure 12. Model three-dimensional trajectory (backward in time from March 5) originating at ($55°N,35°W$) in the atmospheric boundary layer (ABL). Crosses are plotted every 12 hours, pressure labels once per day.

as compared to $NOx_{emission}$ at only 3 pptv. At $55°N,35°W$ the March 5 trajectory (Figure 12) shows that the NO_x originated over the strong emission region of the eastern United States and was rapidly advected north and east near and in the ABL, reaching the North Atlantic at 955 mbar in only 2 days. This rapid transport allowed most of the NO_x to remain as $NOx_{emission}$ without converting to HNO_3 or PAN, while travel in the relatively warm ABL produced ~ 20% of the total NO_x as $NOx_{PANtrans}$.

In the lower latitudes of the eastern Pacific the March 27 trajectory (Figure 13a) indicates a considerably more complicated transport path. The $NOx_{PANtrans}$ pulse at ($30°N,155°W$) began as PAN in the midtroposphere over eastern Asia. After crossing the northern Pacific in the early spring westerlies, it was then subjected to downward motion produced by midlatitude storm systems and subsided anticyclonically southward into the subtropical ABL where it thermally converted to NO_x. This can readily be seen in Figure 13b where we present the mixing ratios of $NOx_{emission}$, $NOx_{PANtrans}$, PAN, and the atmospheric pressure of this trajectory during the last four days before arriving at $30°N,155°W$ (along the x axis, 0 implies March 27; -4 implies March 23). Also, this figure displays only the tracer mixing ratios. It does not illustrate the relative influence of advection or photochemical tendencies on the resulting mixing ratios.

We first note that although $NOx_{emission}$ mixing ratios are small, there is an interesting decrease from 27 pptv to 3 pptv as the parcel moves from $60°N$ to $30°N$ and increasing values of OH convert the NO_x to HNO_3. More importantly, during March 23-25, when the air parcel was slowly sinking from the middle to lower troposphere, both PAN and $NOx_{PANtrans}$ remained essentially constant with high PAN values near 450 pptv and very low $NOx_{PANtrans}$ mixing ratios (~15 pptv). Over the final two days, as the trajectory continued to subside and entered the warm ABL, PAN showed a marked decrease in mixing ratio, while $NOx_{PANtrans}$ exhibited an abrupt increase to a final value of 137 pptv.

This specific NO_x event clearly shows the complex roles played by the sequestering of PAN in the colder regions of the troposphere and subsequent transport southward and downward, resulting in a significant redistribution of NO_x. This type of process can also be seen in the central North Atlantic Ocean (not shown); however, the influence of the

United States and European emission regions results in a stronger impact by $NOx_{emission}$, although $NOx_{PANtrans}$ dominates. One should also note that the release of NO_x from subsiding PAN due to synoptic scale storms also occurs over midlatitude continental regions. However, its contribution is typically masked by large NO_x emissions in the ABL.

4.4. Influence of Subsiding PAN on Oceanic NO_x

Thus far, our model analysis of PAN's long-range transport and its subsequent decomposition to NO_x in warmer regions of the ABL has revealed that its greatest effect is seen in the NH oceanic subtropics during winter and spring (factor of 5) with less of an impact in middle and high latitudes (factor of 2). Furthermore, local examination of surface grid points has indicated that dynamical sinking of PAN from the free troposphere plays a significant role. To tie together these results, it would be informative to quantify the regional and seasonal levels of NO_x released as a result of subsiding PAN as opposed to the sum of $NOx_{emission}$ and NO_x released from PAN that was advected only in the ABL. To accomplish this, we designed an experiment which allowed PAN chemistry to take place only in the model's ABL (bottom two levels). Any PAN transported into or chemically produced in the free troposphere was removed at a maximum rate that insured numerical stability, while all the remaining chemistry was
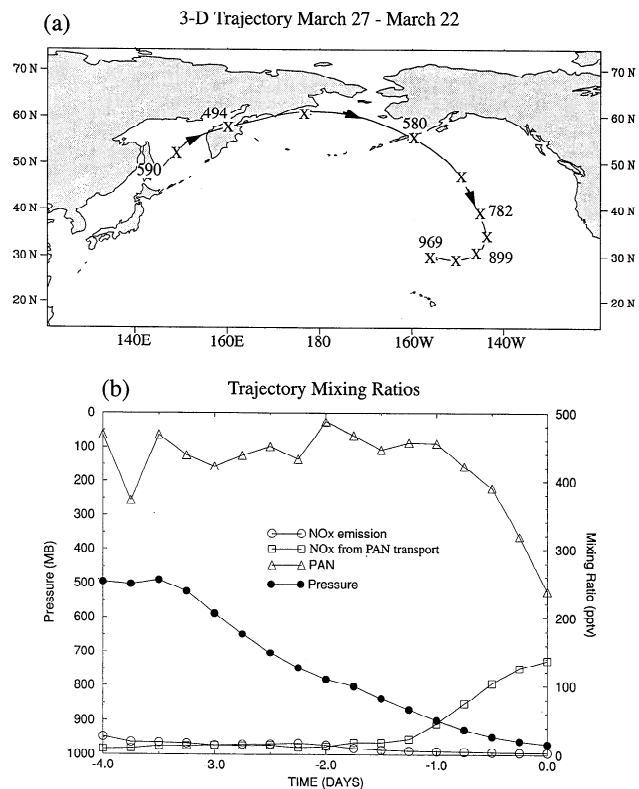
Figure 13. (a) Model three-dimensional trajectory (backward in time from March 27) originating at ($30°N,155°W$) in the ABL. Crosses are plotted every 12 hours, pressure labels (mbar) once per day. (b) Mixing ratios (pptv) for $NOx_{emissions}$, $NOx_{PANtrans}$ and PAN and the vertical location (mbar) of the trajectory depicted in Figure 12a. Values are plotted backward in time every six hours. Along the x axis, 0 implies March 27 at ($30°N,155°W$) and -4 implies March 23 north of Japan.

NOx From Free Trop PAN / NOx From Full Chem
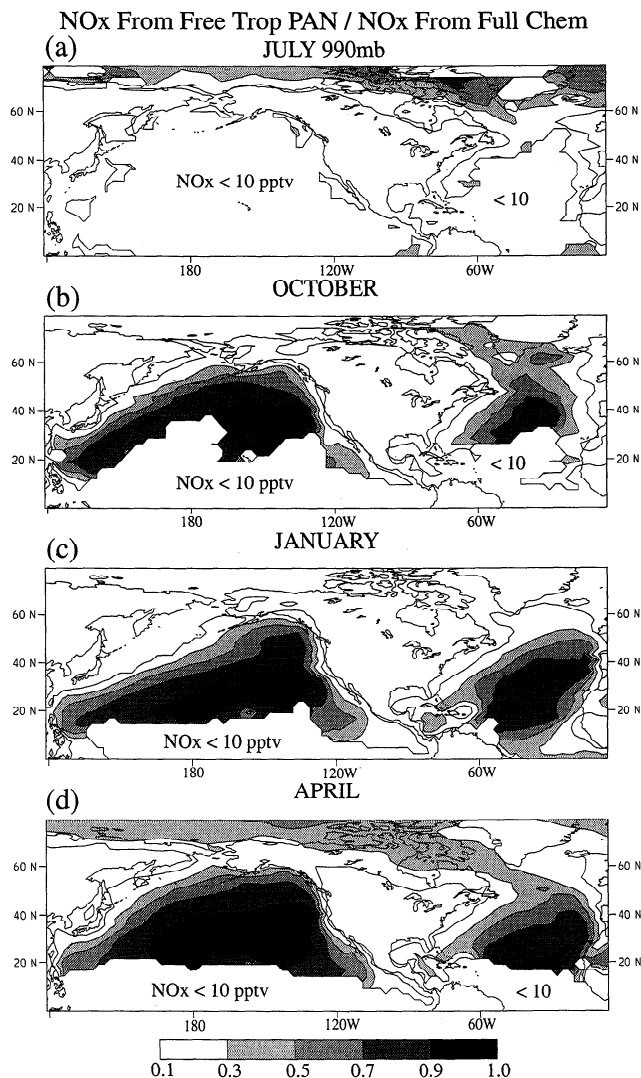
Figure 14. Ratio at 990 mbar of NO_x released from subsiding PAN to NO_x from complete transport and chemistry for (a) July, (b) October, (c) January, and (d) April. Ratios were not plotted for largest local NO_x values less than 10 pptv.

identical to the original integration. To obtain fields of NO_x which were released only from PAN that subsided into the ABL, we simply subtracted the results of this experiment from the original complete chemistry experiment.

In Figure 14 we present the 990 mbar ratio of NO_x from free tropospheric PAN to NO_x from complete chemistry during July, October, January, and April for NO_x values greater than 10 pptv in the NH. Overall, we see that subsiding PAN accounts for most of the NO_x found over more than half of the Pacific and Atlantic Oceans during winter and spring, while there is essentially no contribution during summer and an onset of NO_x release in the midlatitude oceans during autumn. Near the east coasts of Asia and North America, prevailing westerly offshore winds transport NO_x and PAN directly from emission regions in the ABL, overwhelming any contribution from subsiding PAN decomposition. A closer examination of this ratio begins to clarify and bind together the interactions of meteorological transport, tropospheric temperature, and source regions of NO_x and PAN, discussed in previous sec-

tions, that produce the resulting NO_x distributions over remote regions of the oceanic ABL.

The basic transport mechanism involves the midlatitude baroclinic storm systems driven by the strong north to south temperature gradients seen from late fall through spring. As described in section 3.4, these transient cyclones transport ABL air upward and northward on their downstream side and free tropospheric air downward and southward behind them as they typically move to the east and north, reaching their southernmost influence from winter through early spring.

As seen in Figures 14a and 14b, tropospheric PAN storage and baroclinic storms are at a minimum during the warmth of summer and there is essentially no contribution to surface NO_x from subsiding PAN. However, as autumn approaches, cooling temperatures and early baroclinic transport begins to sequester PAN aloft as well as affect the higher latitudes of the ocean regions where surface temperatures are still warm enough to decompose PAN. In winter (Figure 14c), as the baroclinic storms intensify, their influence is felt well into the subtropics with a 70% subsidence effect over most of the ocean south of $40°N$. It is interesting to note that over the Northwest Pacific there is no contribution to NO_x from sinking PAN even though this is an area of intense winter storms. This is a consequence of very cold surface temperatures being advected off the Asian continent producing long PAN lifetimes. In addition, the high NO_x mixing ratios simulated in this region [see H. Levy II et al. (manuscript in preparation, 1996)] result from a low solar angle producing a slow winter NO_x chemistry which allows the surface transport of NO_x from Asian emissions to the North Pacific before conversion to HNO_3.

In spring (Figure 14d), NO_x from subsiding PAN reaches its maximum in the Pacific where shorter PAN and NO_x lifetimes have allowed its influence to spread northwestward. As a result of warming spring temperatures, we also observe the appearance of a greater than 30% band in the polar region which lasts into summer. Singh et al. [1992b], using ABLE 3A summer measurements from Alaska and a one-dimensional chemical model run to equilibrium, speculated that 50 to 70% of the median NO_x mixing ratios observed could have come from the PAN reservoir. Also, similar calculations [Singh et al., 1994] utilizing ABLE 3B data over eastern Canada suggested that 15 to 20 pptv of NO_x could have resulted from PAN. An analysis our of model meteorology depicted subsidence occurring in this area from late autumn into late spring, providing an influx of sequestered PAN to the Arctic ABL where NO_x could be released with the advent of sufficiently warm temperatures. Although we found that this transport produced only 30-50% of our model NO_x, further examination revealed that within this belt, ABL NO_x consisted of roughly equal amounts of NO_x produced by subsiding PAN, NO_x produced by PAN that formed and decomposed only in the ABL, and $NO_{x\text{emission}}$. Farther south over Canada, $NO_{x\text{emission}}$ from combustion source regions begins to dominate NO_x.

5. Summary

Using the GFDL three-dimensional global chemical transport model with all known emission sources of NO_x, off-line chemistry, and no diurnal cycle, we have simulated the global distribution of PAN, most of which is found in the NH. In the ABL, PAN is concentrated over continental sites of NO_x

emissions, while it is distributed relatively zonally in the free troposphere. In the NH, PAN accumulates in the coldest regions, generally the highest latitudes and altitudes, while in the SH free troposphere, the maximum PAN levels are found in an equator to 30°S belt stretching from South America to Australia. We find that overall, the simulated distribution and available observations generally agree.

On a global tropospheric scale, PAN chemistry has little influence on NO_x, however, its regional affects are significant. Through analysis of a series of numerical experiments, we reach the following conclusions regarding the impact of PAN chemistry and transport on the distribution of tropospheric NO_x: (1) By transferring NO_x from its point of emission to remote regions of the globe, PAN impacts the global distribution of tropospheric NO_x, as was earlier hypothesized by *Crutzen* [1979] and *Singh and Hanst* [1981]. (2) While NO_x levels decline slightly in the source regions, where they are already quite high, NO_x levels in the remote, primarily oceanic regions of the lower troposphere, generally increase by a factor of 2 and in some cases by as much as a factor of 5 during the winter and spring of both hemispheres. This increase suggests a possible transient shift in the chemistry of many of the remote regions of the NH lower troposphere from net ozone destruction to either ozone neutral or ozone production. (3) On the other hand, in the cold upper troposphere where PAN lifetimes are long, PAN chemistry has only a minimal impact on NO_x ($\pm$ 10%). (4) While no general spring maximum is observed in the global tropospheric monthly mean NO_x, spring maxima are observed regionally in the lower troposphere over the North Atlantic at 55°N and 35°N and the eastern Pacific at 30°N. This is generally consistent with an earlier hypothesis of *Penkett and Brice* [1986]. (5) Local time series and trajectory analysis in these remote regions show that the transport producing the monthly mean spring peaks in NO_x is both complex and diverse. At both high and low latitudes the monthly mean consists of many high-magnitude NO_x episodes. These events are large enough to provide periods of ozone production even though the monthly mean value would imply ozone destruction. At high latitudes the early spring peaks are strongly dominated by transport in the ABL of unconverted NO_x from the eastern U. S. emission region. As tropospheric temperatures warm, NO_x from transported PAN begins to prevail. At lower subtropical latitudes, however, NO_x from transported PAN completely dominates. (6) In addition to transporting PAN northward and upward to higher latitudes and longer lifetimes, midlatitude storm systems also provide a complex transport path which carries PAN from the high-latitude midtroposphere of the North Pacific and Atlantic anticyclonically southward and downward to the warm ABL where the PAN is thermally converted to NO_x. From late fall through spring this process provides more than 70% of the ABL NO_x found over half the area of the NH ocean regions.

References

Barrie, L. A., and J. W. Bottenheim, Sulfur and nitrogen pollution in the Arctic atmosphere, in *Pollution of the Arctic Atmosphere,* edited by W.T. Sturges, pp.155-183, Elsevier Sci., New York, 1991.

Benkovitz, C. M., M. T. Scholtz, J. Dignon, J. Pacyna, L. Tarrason, E. C. Voldner. P. A. Spiro, J. A. Logan, and T. E. Graedel, Global gridded inventories of anthropogenic emissions of sulfur and nitrogen, *J. Geophys. Res.,* in press, 1996.

Carlson, T. N., Airflow through midlatitude cyclones and the comma cloud pattern, *Mon. Weather Rev., 108,* 1498-1509, 1980.

Carroll, M. A., et. al., Aircraft measurements of NO_x over the eastern Pacific and continental United States and implications for ozone production, *J. Geophys. Res., 95,* 10,205-10,233, 1990.

Chameides, W. L., and A. Tan, The two-dimensional diagnostic model for tropospheric OH An uncertainty analysis, *J. Geophys. Res., 86,* 5209-5223, 1981.

Chameides, W. L., and J. C. G. Walker, A photochemical theory of tropospheric ozone, *J. Geophys. Res., 78,* 8751-8759, 1973.

Chameides, W. L., D. D. Davis, M. O. Rogers, J. Bradshaw, and S. Sandholm, Net ozone photochemical production over the eastern and central North Pacific as inferred from GTE/CITE 1 observations during fall 1983, *J. Geophys. Res., 92,* 2131-2152, 1987.

Chameides, W. L., et al., Ozone precursor relationships in the ambient atmosphere, *Geophys. Res., 97,* 6037-6055, 1992.

Crutzen, P. J., Photochemical reaction initiated by and influencing ozone in unpolluted tropospheric air, *Tellus, 26,* 45-55, 1974.

Crutzen, P. J., The role of NO and NO_2 in the chemistry of the troposphere and stratosphere, *Ann. Rev. Earth Planet. Sci., 7,* 443-472, 1979.

Crutzen, P. J., Tropospheric ozone: An overview, in *Tropospheric Ozone,* edited by I.S.A. Isaksen, pp. 3-32, D. Reidel, Norwell, Mass., 1988.

Fehsenfeld, F.C., D.D. Parrish, and D.W. Fahey, The measurement of NO_x in the non-urban troposphere, in *Tropospheric Ozone,* edited by I.S.A. Isaksen, pp. 185-216, D. Reidel, Norwell, Mass., 1988.

Iverson, T., Meteorology and transport of air masses in Arctic regions, in *The Tropospheric Chemistry of Ozone in the Polar Regions,* edited by H. Niki and K. H. Becker, pp. 57-75, Springer-Verlag, New York, 1993.

Kanakidou, M., H. B. Singh, K. M. Valentin, and P. J. Crutzen, A two-dimensional study of ethane and propane oxidation in the troposphere, *J. Geophys. Res., 96,* 15,395-15,425, 1991.

Kasibhatla, P. S., NO_y from sub-sonic aircraft emissions: A global three-dimensional model study, *Geophys. Res. Lett., 20,* 1707-1710, 1993.

Kasibhatla, P. S., H. Levy II, W. J. Moxim, and W. L. Chameides, The relative impact of stratospheric photochemical production on tropospheric NO_y levels: A model study, *J. Geophys. Res., 96,* 18,631-18,646, 1991.

Kasibhatla, P. S., H. Levy II, and W. J. Moxim, Global NO_x, HNO_3, PAN, and NO_y distributions from fossil-fuel combustion emissions: A model study, *J. Geophys. Res., 98,* 7165-7180, 1993.

Levy, H., II, Normal atmosphere: Large radical and formaldehyde concentrations predicted, *Science, 173,* 141-143, 1971.

Levy, H., II, and W. J. Moxim, Simulated global distribution and deposition of reactive nitrogen emitted by fossil fuel combustion, *Tellus, 41,* 256-271, 1989.

Levy, H., II, J. D. Mahlman, and W. J. Moxim, Tropospheric N_2O variability, *J. Geophys. Res., 87,* 3061-3080, 1982.

Levy, H., II, J. D. Mahlman, W. J. Moxim, and S. C. Liu, Tropospheric ozone: The role of transport, *J. Geophys. Res., 90,* 3753-3772, 1985.

Levy, H., II, W. J. Moxim, P. S. Kasibhatla, and J. A. Logan, The global impact of biomass burning on tropospheric reactive nitrogen, in *Global Biomass Burning: Atmospheric, Climatic, and Biospheric Implications,* edited by J. S. Levine, pp. 363-369, MIT Press, Cambridge, Mass., 1991.

Levy, H., II, W. J. Moxim, and P. S. Kasibhatla, A global three-dimensional time-dependent lightning source of NO_x, *J. Geophys. Res.,* in press, 1996.

Lin, X., M. Trainer, and S.C. Liu, On the nonlinearity of the tropospheric ozone production, *J. Geophys. Res., 93,* 15,879-15,888, 1988.

Liu, S.C., M. McFarland, D. Kley, O. Zafiriou, and B. Huebert, Tropospheric NO_x and O_3 budgets in the equatorial Pacific, *J. Geophys. Res., 88,* 1360-1368, 1983.

Liu, S.C., et al., The study of the photochemistry and ozone budget during the Mauna Loa Observatory Photochemistry Experiment, *J. Geophys. Res., 97,* 10,463-10,471, 1992.

Mahlman, J. D., and W. J. Moxim, Tracer simulation using a global general circulation model: Results from a midlatitude instantaneous source experiment, *J. Atmos. Sci., 35,* 1340-1374, 1978.

Manabe, S., and J. L. Holloway, Jr., The seasonal variation of the hydrologic cycle as simulated by a global model of the atmosphere, *J. Geophys. Res., 80,* 1617-1649, 1975.

Manabe, S., D. G. Hahn, and J. L. Holloway, Jr., The seasonal variation of the tropical circulation as simulated by a global model of the atmosphere, *J. Atmos. Sci., 31,* 43-83, 1974.

Moxim, W. J., Simulated transport of NO_y to Hawaii during August: A synoptic study, *J.Geophys. Res., 95,* 5717-5729, 1990.

Moxim, W. J., H. Levy II, P. S. Kasibhatla, and W. L. Chameides, The impact of anthropogenic and natural NO_x sources on the global distribution of tropospheric reactive nitrogen and the net chemical production of ozone (abstract), *EOS Trans. AGU, 75,* (44), Fall Meet. Suppl., 135, 1994.

Muller, K. P., and J. Rudolph, Measurements of peroxyacetyl nitrate in the marine boundary layer over the Atlantic, *J. Atmos. Chem., 15,* 361-367, 1992.

Penkett, S. A., and K. A. Brice, The spring maximum in photooxidants in the Northern Hemisphere, *Nature, 319,* 655-657, 1986.

Penner, J. E., C. S. Atherton, J. Dignon, S. J. Ghan, J. J. Walton, and S. Hameed, Tropospheric nitrogen: A three-dimensional study of sources, distributions, and deposition, *J. Geophys. Res., 96,* 959-990, 1991.

Ridley, B. A., et al., Measurements and model simulations of the photostationary state during the Mauna Loa Observatory Photochemistry Experiment: Implications for radical concentrations

and ozone production and loss rates, *J. Geophys. Res., 97,* 10,375-10,388, 1992.

Roelofs, G.-J. and J. Lelieveld, Distribution and budget of O_3 in the troposphere calculated with a chemistry general circulation model, *J. Geophys. Res., 100,* 20,983-20,998, 1995.

Shepson, P. B., D. R. Hastie, K. W. So, H. I. Schiff, and P. Wong, Relationships between PAN, PPN, and O_3 at urban and rural sites in Ontario, *Atmos. Environ., 26A,* 1259-1270, 1992.

Sillman, S., J. A. Logan, and S. C. Wofsy, The sensitivity of ozone to nitrogen oxides and hydrocarbons in regional ozone episodes, *J. Geophys. Res., 95,* 1837-1852, 1990.

Singh, H. B., and P. L. Hanst, Peroxyacetyl nitrate [PAN] in the unpolluted atmosphere: An important reservoir for nitrogen oxides, *Geophys. Res. Lett., 8,* 941-944, 1981.

Singh, H. B., L. J. Salas, and W. Viezee, Global distribution of peroxyacetyl nitrate, *Nature, 321,* 588-591, 1986.

Singh, H. B., et al., Atmospheric peroxyacetyl nitrate measurements over the Brazilian Amazon basin during the wet season: Relationships with nitrogen oxides and ozone, *J. Geophys. Res., 95,* 16,945-16,954, 1990a.

Singh, H. B., et al., Peroxyacetyl nitrate measurements during CITE 2: Atmospheric distribution and precursor relationships, *J. Geophys. Res., 95,* 10,163-10,178, 1990b.

Singh, H. B., et al., Atmospheric measurements of peroxyacetyl nitrate and other organic nitrates at high latitudes: Possible sources and sinks, *J. Geophys. Res., 97,* 16,511-16,522, 1992a.

Singh, H. B., D. Herlth, D. O'Hara, K. Zahnle, J. D. Bradshaw, S. T. Sandholm, R. Talbot, P. J. Crutzen, and M. Kanakidou, Relationship of peroxyacetyl nitrate to active and total odd nitrogen at northern high latitudes: Influence of reservoir species on NO_x and O_3, *J. Geophys. Res., 97,* 16,523-16,530, 1992b.

Singh, H. B., et al., Summertime distribution of PAN and other reactive nitrogen species in the northern high-latitude atmosphere of eastern Canada, *J. Geophys. Res., 99,* 1821-1835, 1994.

Trainer, M., et al., Observations and modeling of the reactive nitrogen photochemistry at a rural site, *J. Geophys. Res., 96,* 3045-3063, 1991.

Walega, J. G., et al., Observations of peroxyacetyl nitrate, peroxypropionyl nitrate, methyl nitrate, and ozone during the Mauna Loa Observatory Photochemistry Experiment, *J. Geophys. Res., 97,* 10,311-10,330, 1992.

P. S. Kasibhatla, School of Earth and Atmospheric Sciences, Georgia Institute of Technology, Atlanta, GA 30332. (e-mail: psk@mcnc.org)

H. Levy II and W. J. Moxim (corresponding author), NOAA Geophysical Fluid Dynamics Laboratory, Princeton University, P.O. Box 308, Princeton, NJ 08542. (e-mail: wm@gfdl.gov)